

Provenance, depositional setting and diagenesis as keys to reservoir quality of the Lower Cretaceous in the SW Barents Sea

Angelica Ärlebrand^{a,1}, Carita Augustsson^{a,*}, Alejandro Escalona^a, Sten-Andreas Grundvåg^b, Dora Marín^a

^a Department of Energy Resources, University of Stavanger, 4021, Stavanger, Norway

^b Department of Geosciences, UiT - The Arctic University of Norway, Norway

ARTICLE INFO

Keywords:

Diagenesis
Depositional setting
Provenance
Petrography
Reservoir quality
Petrophysics
Barents sea

ABSTRACT

This study examines the role of the depositional environment for the final reservoir quality in four Lower Cretaceous sandstone reservoirs in the southwestern Barents Sea by linking facies to the distribution of primary textures, composition, and diagenetic alteration. Facies analysis reveals slope-to-basin-floor, distal shallow-marine, and deltaic depositional environments. The slope-to-basin-floor sandstone has the highest porosity of 3–19% (avg. 13%). It is attributed to good sorting, non-pervasive carbonate cementation that inhibited compaction and allowed for secondary porosity through later dissolution, and moderate clay infiltration that resulted in clay cutanes on grain rims and the precipitation of chlorite (which inhibited quartz growth). For the deltaic sandstone, moderate to fluctuating energy and sediment supply provided good conditions for mechanical clay infiltration and varying porosity of 2–18% (avg. 8%). The distal shallow-marine sandstone reservoir has the lowest porosity of 1–12% (avg. 7%). Based on its fine-grained and bioturbated character, deposition in a low-energy environment with low sediment supply seems likely. The combination of fine-grained lamina, interstitial matrix and bioturbation led to porosity reduction. Abundant mica and feldspar grains in the shallow-marine sandstone, partly a result of the provenance, and deep burial also resulted in extensive illitization. High mineralogical maturity, much monocrystalline quartz in the quartz-grain populations, and similar felsic chemical rock compositions for all facies associations and wells indicate similar source rocks with some variations. Abundant mechanically unstable mica makes the nearby Loppa High a plausible catchment, which is supported by the seismic geometries. This study demonstrates that the porosity evolution of the studied Lower Cretaceous sandstone reservoirs is determined mainly by the depositional environment despite minor provenance and major diagenetic variations.

1. Introduction

Successful exploration of prolific sandstone reservoirs largely depends on correct interpretation of the depositional setting and understanding of the link between provenance, depositional conditions, diagenesis, and the resulting reservoir quality (e.g., Dickinson and Suczek, 1979; Morad et al., 2010; Bjørlykke, 2014). Alas, most published studies on reservoir-quality factors focus on only a part of the sedimentological cycle (erosion and transport, deposition, diagenesis and uplift; some noble exceptions are Ramm, 2000; Reed et al., 2005; Gutiérrez Paredes et al., 2018). For the Lower Cretaceous sandstone

units in the southwestern Barents Sea, which are the focus of this study, only few publications have investigated the sedimentological and petrographic properties to reveal depositional and reservoir conditions (e.g., Edwards, 1979; Marín et al., 2018a).

Upper Jurassic to Lower Cretaceous wedges along rift-faulted basin margins are considered valid petroleum plays in the southwestern Barents Sea, but the quality of the reservoirs varies and often is lower than expected despite shallow maximum burial depths (in the order of 2000–3000 m before Cenozoic uplift; Henriksen et al., 2011; Baig et al., 2016; Ktenas et al., 2019). The depositional environments for this syn-rift-deposited sand have been suggested to span from deltaic to

* Corresponding author.

E-mail addresses: a.arlebrand@gmail.com (A. Ärlebrand), carita.augustsson@uis.no (C. Augustsson), alejandro.escalona@uis.no (A. Escalona), sten-andreas.grundvag@uit.no (S.-A. Grundvåg), dora.l.restrepo@uis.no (D. Marín).

¹ Present address: Luossavaara-Kirunavaara AB, Sweden.

<https://doi.org/10.1016/j.marpetgeo.2021.105217>

Received 5 October 2020; Received in revised form 30 June 2021; Accepted 1 July 2021

Available online 6 July 2021

0264-8172/© 2021 The Author(s). Published by Elsevier Ltd. This is an open access article under the CC BY license (<http://creativecommons.org/licenses/by/4.0/>).

shoreface and submarine-fan settings (Stewart et al., 1995; Seldal, 2005; Iqbal, 2016; Marín et al., 2018a, 2018b). Previous work suggests sediment transport from locally uplifted highs (e.g., Gabrielsen et al., 1990; Seldal, 2005; Marín et al., 2018a). The general low reservoir quality has been linked to diagenesis as a result of initial deep burial followed by extensive uplift and erosion of more than 1000 m of sedimentary strata during the Cenozoic Era (Henriksen et al., 2011); provenance and depositional settings have not been taken into account. Consequently, little is known about the link between the reservoir quality and the provenance and depositional environments of the Lower Cretaceous sandstone.

The main purpose of this study is to determine how different sedimentary facies and depositional environments control reservoir quality in the southwestern Barents Sea. To achieve this, four Lower Cretaceous sandstone-bearing reservoirs at the southern and western margin of the Loppa High (Fig. 1) are compared in terms of sedimentary facies, texture, composition, provenance, and ultimately reservoir properties. Core descriptions are combined with thin-section analysis. X-ray diffraction (XRD) and geochemical data are used to aid mineral identification and provenance analysis. Seismic and well-log data highlight the stratigraphic and structural framework.

2. Lower Cretaceous tectonic-stratigraphic framework

After a tectonically relatively quiet early Mesozoic phase in the southwestern Barents Sea, tectonic activity increased during Late Jurassic time and culminated during Early Cretaceous time (Doré, 1995; Worsley, 2008; Blaich et al., 2017; Serck et al., 2017). Widespread rifting, local inversion and strike-slip faulting along older structural lineaments caused differential basin subsidence and uplift, which led to formation of the present-day structural arrangement of platforms, basins and highs (Gabrielsen et al., 1990; Faleide et al., 1993, 2018).

The western margin of the Loppa High is bound by the Bjørnøyrenna Fault Complex and the Ringvassøy-Loppa Fault Complex further south (Fig. 1). The Asterias Fault Complex marks the border towards the Hammerfest Basin in the south (Fig. 1). The southwestern flank of the Loppa High was subject to recurrent rift-shoulder uplift during

Valanginian to Barremian time with less activity along the Asterias Fault Complex than the Bjørnøyrenna Fault Complex (Indrevær et al., 2017; Marín et al., 2018a). Following a distinct early Aptian rift phase (Blaich et al., 2017), the rift activity decreased and shifted focus towards the north with faulting in the Fingerdjupet Subbasin northwest of the Loppa High (Fig. 1) after early Albian time (Serck et al., 2017; Kairanov et al., 2019). Tilting of the high during late Aptian to early Albian time led to a steep slope on the western flank and a more gentle slope on the eastern side (Marín et al., 2018a; Kairanov et al., 2019).

The Lower Cretaceous succession of the southwestern Barents Sea is divided into the Knurr, Kolje, and Kolmule formations (Fig. 2). The deposits consist mainly of mudstone-dominated units of deep-shelf origin, and sandstone-rich wedges occur along the flanks of structural highs and along major fault zones (Fig. 2; Richardsen et al., 1993; Mørk et al., 1999; Halland et al., 2014). Locally uplifted highs acted as source areas for the coarse-grained material, which was deposited in fluviodeltaic, shallow-marine, and slope-to-basin-floor environments (Seldal, 2005; Sattar et al., 2017; Corseri et al., 2018; Marín et al., 2018a, 2018b). Large southeastward prograding fluviodeltaic systems also supplied sediment to the basins, particularly during Barremian time (e.g., Grundvåg et al., 2017; Midtkandal et al., 2020).

This study pertains to four wells that proved gas in Aptian to Albian strata in the Hammerfest Basin and along the nearby margins of the Loppa High (Fig. 1). Iqbal (2016) and Marín et al. (2018b) suggested a slope-channel setting, possibly related to an up-dip fan delta, for the Skalle-well reservoir (7120/2-3S) and a submarine fan for the Juksa-well reservoir (7120/6-3S); both wells are located near the Asterias Fault Complex (Fig. 1). Rock-physical data gave porosity values of 7–27% for the Skalle-well reservoir (7120/2-3S; Iqbal, 2016). A storm-affected offshore to distal shoreface environment is suggested for the Salina-well reservoir (7220/10–1) near the Ringvassøy-Loppa Fault Complex (Marín et al., 2018a, Fig. 1). No study on the depositional environment of the Nunatak well (7220/5–2) at the Bjørnøyrenna Fault Complex (Fig. 1) has been published to date. The lateral variability of the deposits led Marín et al. (2017, 2018b) to define seven third-order genetic sequences (S0–S6; Fig. 2) in the study area. The reservoirs of the Juksa (7120/6-3S), Skalle (7120/2-3S) and Nunatak (7220/5–2)

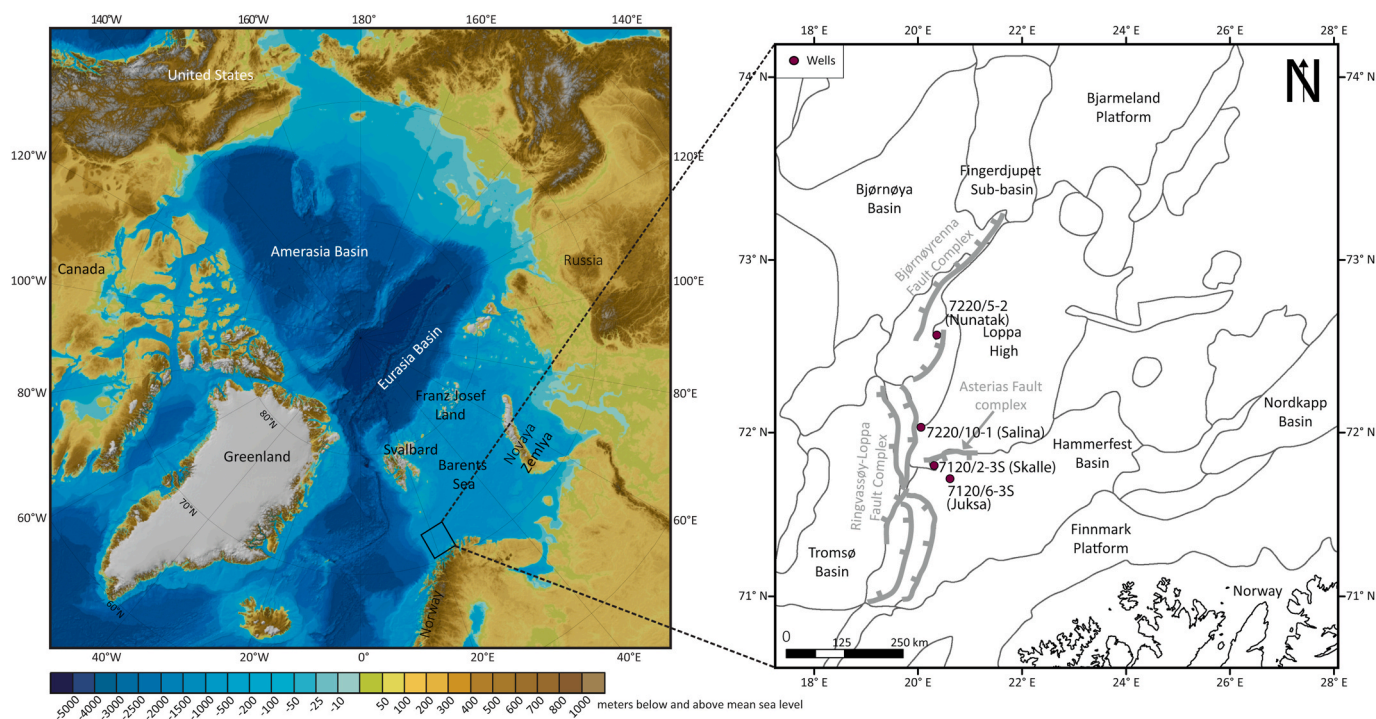


Fig. 1. Location of the study area and studied wells in the southwestern Barents Sea (bathymetric map from Jakobssen et al., 2012). The Fault Complexes are simplified from Marín et al. (2018a).

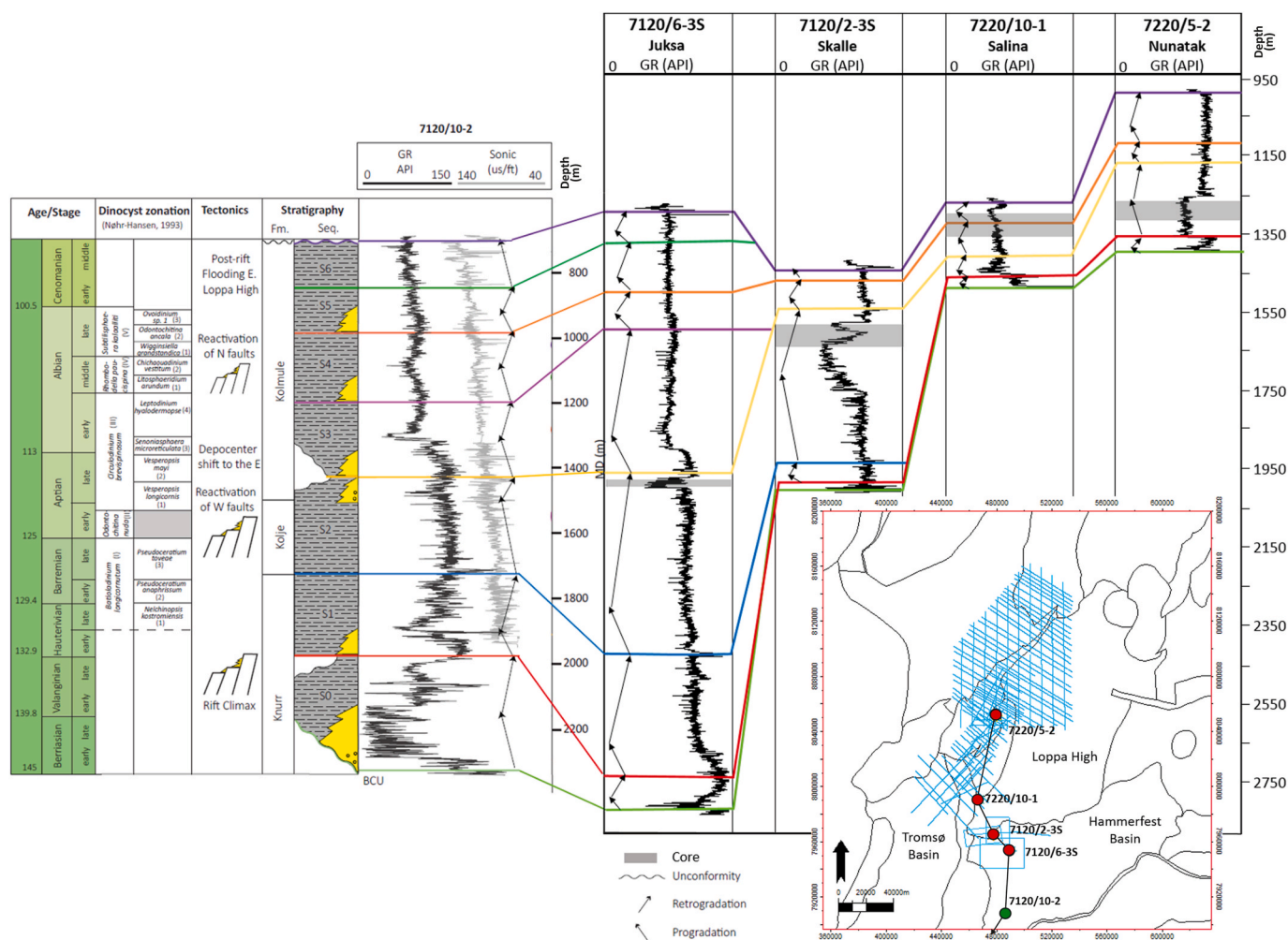


Fig. 2. Early Cretaceous to Cenomanian stratigraphy including gamma-ray (GR) correlation of depositional sequences (seq.; Marín et al., 2018b) from the reference well 7120/10-2 (outside the map in the Hammerfest basin) to the four wells in this study. The dinoflagellate cyst (dinocyst) biostratigraphy is from Nøhr-Hansen (1993): Ov = *Ovoidinium* sp. 1, Od = *Odontochitina ancala*, Wi = *Wigginsella grandstandica*, Ch = *Chichaouadinium vestitum*, Li = *Litosphaeridium arundum*, Le = *Leptodinium hyalodermopse*, Se = *Senoniasphaera microreticulata*, Vem = *Vesperopsis mayi*, Vel = *Vesperopsis longicornis*, Pst = *Pseudoceratium toveae*, Psa = *Pseudoceratium anaphrissum*, Ne = *Nelchinopsis kostromiensis*. The straight lines in the inset illustrate the available seismic data.

wells are located in the Aptian part of S2, whereas the Salina-well reservoir (7220–10/1) encompasses Albian strata spanning the S4–S5 transition (Fig. 2).

3. Data and methods

The data set includes well logs, 174 m of conventional cores, thin sections, XRD, and geochemical data from the Skalle (7120/2-3S), Juksa (7120/6-3S), Nunatak (7220/5-2) and Salina (7220/10-1) wells (Fig. 1). In addition, we investigated publicly available 2D and 3D seismic data from the Norwegian DISKOS database (Fig. 2). The detailed methodology is provided in Supplementary material S1; only brief information is given here.

For the cored intervals of the Juksa (7120/6-3S), Skalle (7120/2-3S), and Nunatak (7220/5-2) wells, seventeen lithofacies (F1–F17; Supplementary material S2) were recognized and grouped into six facies associations (FA1–FA6; Fig. 3; supplementary materials S1 and S3). For the Salina well (7220/10-1), sedimentological descriptions and facies-association interpretations of Marín et al. (2018a) were adopted. Synthetic seismograms were generated from sonic and density logs to compare wells and seismic data. Five seismic facies were defined and correlated with the core sections. The seismic facies were used to map the extent and distribution of the interpreted depositional systems. Fifty

thin sections of sandstone (ten from Juksa, 7120/6-3S, eighteen from Skalle, 7120/2-3S, seven from Salina, 7220/10-1, fifteen from Nunatak, 7220/5-2) were analyzed with a polarizing microscope (Supplementary material S4). Three bulk samples from each of the Juksa (7120/6-3S), Salina (7220/10-1), and Nunatak wells (7220/5-2), and six from the Skalle well (7120/2-3S) were used for XRD analysis. Seven sandstone samples from the Juksa well (7120/6-3S), ten from the Salina well (7220/10-1), and thirteen samples each from the Nunatak (7220/5-2) and Skalle (7120/2-3S) wells were analyzed for the whole-rock element-chemical composition (Supplementary material S5).

4. Facies associations and depositional environments

The facies associations are described in Supplementary material S1 (and as table in Supplementary material S3); only interpretative descriptions are given here.

4.1. Slope-to-basin-floor facies associations (FA1, FA2)

The slope-to-basin-floor succession includes slope-channel (FA1) and basin-floor-fan deposits (FA2). They occur at the southern flank of the Loppa High, extending into the Hammerfest Basin. Their seismic data exhibit high amplitudes with a distribution that generally is irregular

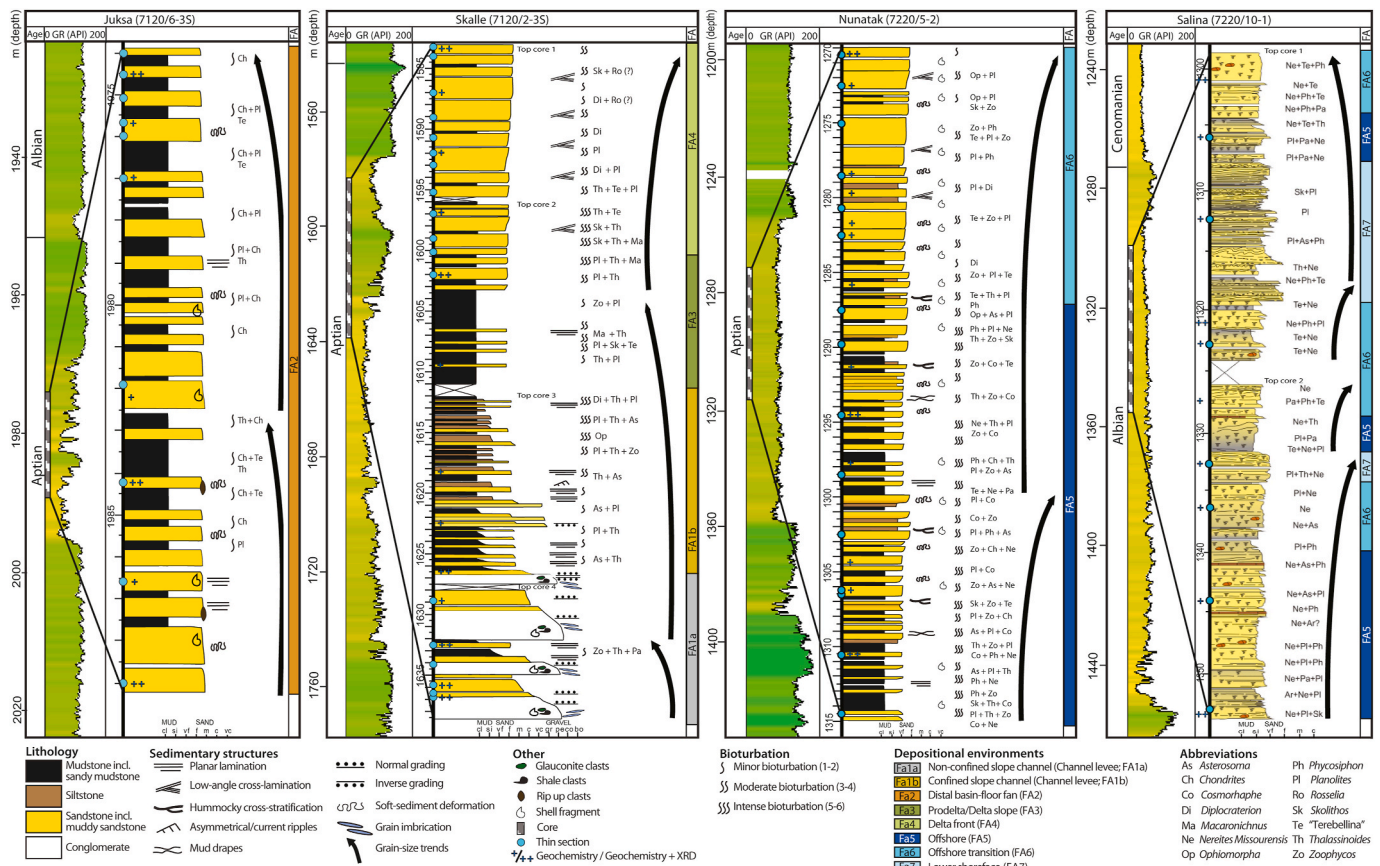


Fig. 3. Sedimentological and gamma-ray (GR) logs for the Lower Cretaceous succession of the four studied wells, including facies associations (FA). The lithological log (including colours) and facies-association interpretation for the Salina well (7220/10-1) are from [Marín et al. \(2018a\)](#). The bioturbation-intensity index is from [Taylor and Goldring \(1993\)](#) and ages base on [Marín et al. \(2018a\)](#). (For interpretation of the references to colour in this figure legend, the reader is referred to the Web version of this article.)

and patchy proximal to the Loppa High (Figs. 4 and 5).

The slope-channel deposits (FA1; 26 m of cores in the Skalle well, 7120/2-3S) are characterized by low textural maturity, partly imbricated basal conglomerate and inversely graded pebbly sandstone beds (Fig. 6A, B, C, D) that indicate short transport and rapid deposition by flows of high sediment concentration, possibly from slope-failure-triggered debris flows and high-density turbidity currents (cf. [Lowe, 1982](#)). Mudstone and siltstone interbeds with trace fossils may represent background deposition by suspension settling and diluted low-density turbidity currents, respectively. Alternation between sandstone and finer-grained beds in the upper part of the FA1 succession suggests low-energy deposition, sporadically interrupted by passing turbidity flows (cf. [Beaubouef et al., 1999](#)). The ichnofauna represents a mixture of shallow-water and deep-water organisms typical of a mass-flow-influenced environment ([Seilacher, 1967](#); [Shanmugam et al., 1994](#); [MacEachern and Bann, 2008](#)). Rapidly decreasing gamma-ray values followed by increasing to stable patterns (Table 1, Fig. 3) probably reflect an erosional unconformity resulting from slope failure and the scouring and infill of a slope-channel complex. Moderate to high amplitude wedge-shaped, discontinuous and sometimes chaotic seismic reflections that onlap towards the Loppa High and downlap onto the underlying surface (Table 1, Fig. 4) are in accordance with a slope-channel interpretation. Similarly, [Marín et al. \(2018b\)](#) suggested a slope-channel environment for the Lower Cretaceous reservoir succession in the Skalle well (7120/2-3S).

The basin-floor-fan deposits (FA2; 15 m of cores in the Juksa well, 7120/6-3S) include massive to laminated sandstone beds with rip-up clasts and load structures that resemble Bouma divisions $T_{a/b}$ and indicate deposition from low-density turbidity currents. Alternation with

thick, black, structureless mudstone layers (Fig. 6E and F) that include pyritized trace fossils indicates longer periods of anoxic and low-energy conditions, possibly below the storm-weather wave base (cf. [Löwenmark, 2007](#); [Ohkouchi et al., 2015](#)). This is typical for the distal lobes of submarine fans (cf. [Mutti and Ricci Lucchi, 1972](#); [Shanmugam et al., 1985](#)). Serrated gamma-ray values represent alternating lithologies in the cores. Increasing values towards the top (Table 1, Fig. 3) record the thinning-upwards of sandstone beds in the core. Laterally continuous seismic reflectors that extend for several kilometers into the basin and gradual thicken towards the slope-channel facies association (FA1; Table 1, Figs. 4 and 5) suggest a basin-floor-fan setting, in accordance with the interpretation of [Marín et al. \(2018b\)](#).

4.2. Deltaic facies associations (FA3, FA4)

The deltaic facies associations include delta-slope/prodelta (FA3) and delta-front environments (FA4). The deltaic seismic facies occurs as lobes at the southern flank of the Loppa High, extending and thinning into the Hammerfest Basin over distances of about 10 km (Fig. 4).

The delta-slope/prodelta deposits (FA3; 11 m of cores in the Skalle well, 7120/2-3S) contain intensely bioturbated mudstone (Fig. 6G) that indicates a well-oxygenated environment with low rates of sedimentation at fair-weather conditions ([MacEachern and Bann, 2008](#)). The trace fossils *Skolithos*, *Macaronichnus* and *Diplocraterion* and overlying glauconitic sandstone (Fig. 6G and H) indicate shallow-marine conditions and reduced sedimentation rates (cf. [Seilacher, 1967](#); [MacEachern and Bann, 2008](#)). Transition from FA1 to FA3 is marked by increasing gamma-ray values reflecting a change from high-energy to low-energy conditions (Table 1). Upwards decreasing gamma-ray values (Fig. 3)

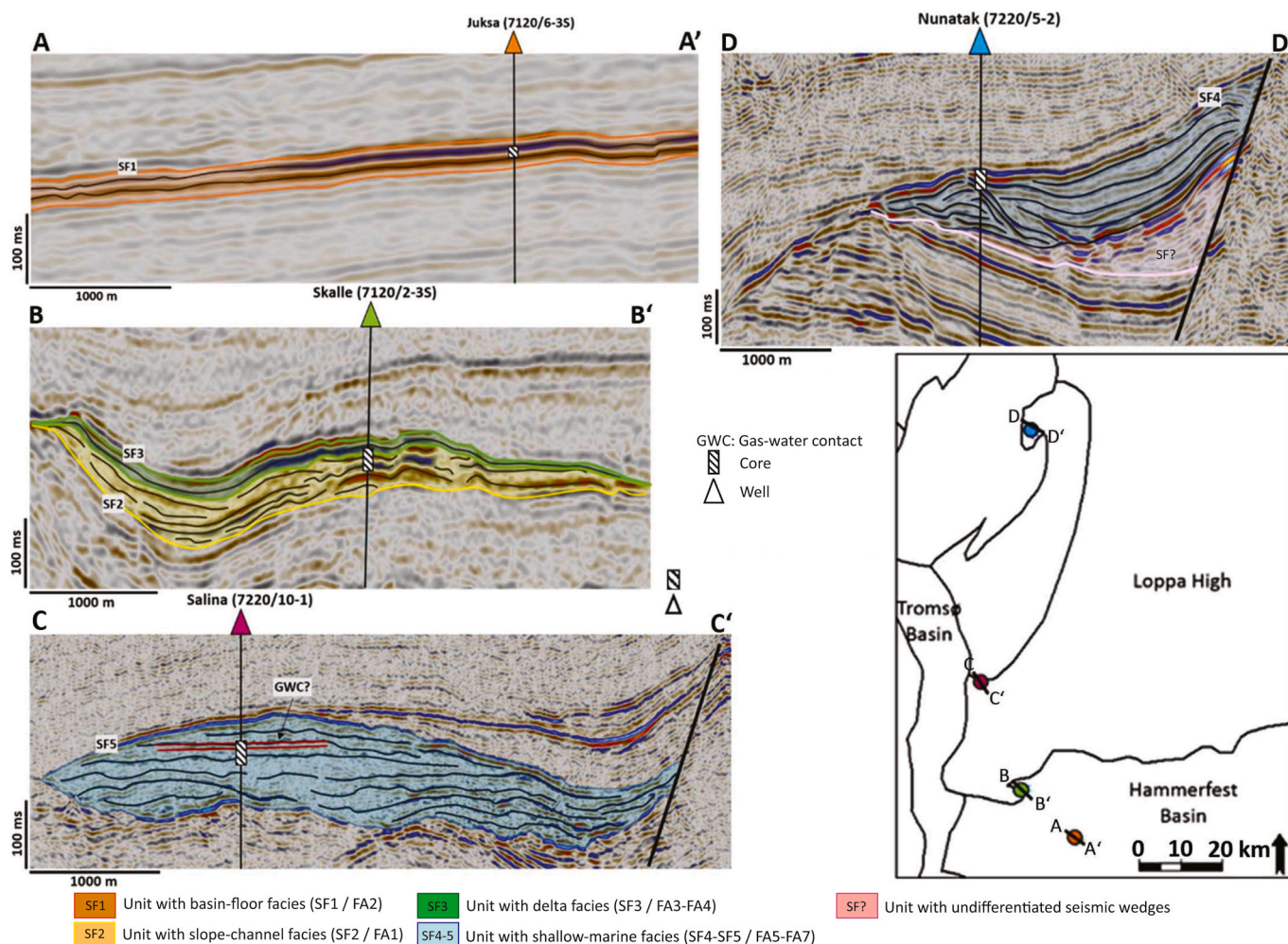


Fig. 4. Seismic lines with seismic facies of the different depositional environments. Horizontal lines (red) in the shallow-marine facies of the Salina well (7220/10–1) possibly represent the gas-water contact. The Nunatak (7220/5–2) and Salina wells are projected and the exact position of the cores may differ slightly from marked locations. (For interpretation of the references to colour in this figure legend, the reader is referred to the Web version of this article.)

probably record a grain-size increase due to delta progradation. Downlapping reflectors may thus represent delta foresets (cf. Gani and Bhattacharya, 2005; Enge et al., 2010; Gobo et al., 2015). This interpretation is supported by the existence of fan deltas south of the Loppa High during Valanginian time and possibly also during the Aptian (Iqbal, 2016; Marin et al., 2018b).

Sandstone-rich delta-front deposits (FA4; 18 m of cores in the Skalle well, 7120/2-3S) exhibit cross-stratification and a low degree of bioturbation (Fig. 3). Collectively, this indicates deposition by traction processes at increased energy conditions and sedimentation rates (cf. MacEachern and Bann, 2008). The trace-fossil suite corresponds to a mixed *Skolithos-Cruziana* ichnofacies association, indicating a mixed moderate-energy to high-energy, open-marine setting (Seilacher, 1967; MacEachern and Bann, 2008). Thus, in combination with the upwards coarsening and seismic downlapping reflectors, FA4 is interpreted to record either the progradation of a delta front or a shallow-marine system. An abrupt increase in gamma-ray values above the FA4-section top (Table 1, Figs. 3 and 5) probably represents a major flooding event.

4.3. Shallow-marine facies associations (FA5, FA6, FA7)

The shallow-marine facies associations include deposits of offshore (FA5), offshore transition (FA6), and lower shoreface origin (FA7). The succession extends for ca. 30 km along the western flank of the Loppa

High and significant depocenters typically are located in the deepest parts of graben structures (up to 300 ms thick; Figs. 4 and 5). The overall shallow-marine facies associations are characterized by wedge-shaped low-amplitude, continuous to sub-continuous parallel reflections (Figs. 4 and 5).

The offshore deposits (FA5; 28 m of core in Nunatak, 7220/5–2; ca. 22 m core in Salina, 7220/10–1) contain a trace-fossil suite that corresponds to mixed high-diversity *Zoophycos*, *Cruziana*, and *Nereites* ichnofacies assemblages (Fig. 6I and J) that are common in slope to distal lower shoreface environments (Seilacher, 1967; MacEachern and Bann, 2008). Overlapping trace-fossil assemblages, intense bioturbation, and a dominance of mudstone (Fig. 6I, J, K) also demonstrate progressively lower-energetic, distal-marine environment mainly below storm-wave base with low sedimentation rates mostly with settling of suspended load (e.g., MacEachern and Bann, 2008). Observed low-angle lamination resembles hummocky cross stratification (Fig. 6L). Together with randomly oriented shell fragments, this indicates frequent reworking by major storms. Heterolithic bedding with mudstone drapes and load structures (Fig. 6M) may indicate cyclic deposition by tidal or low-density turbidity currents immediately below the storm-wave base (e.g., Dashtgard et al., 2012). Stacked upward coarsening trends and increasing gamma-ray patterns (Table 1, Fig. 3) indicate repeated cycles of progradation and shallowing.

The offshore-transition deposits (FA6; 17 m of cores in Nunatak, 7220/5–2; ca. 21 m in Salina, 7220/10–1) include a trace-fossil suite

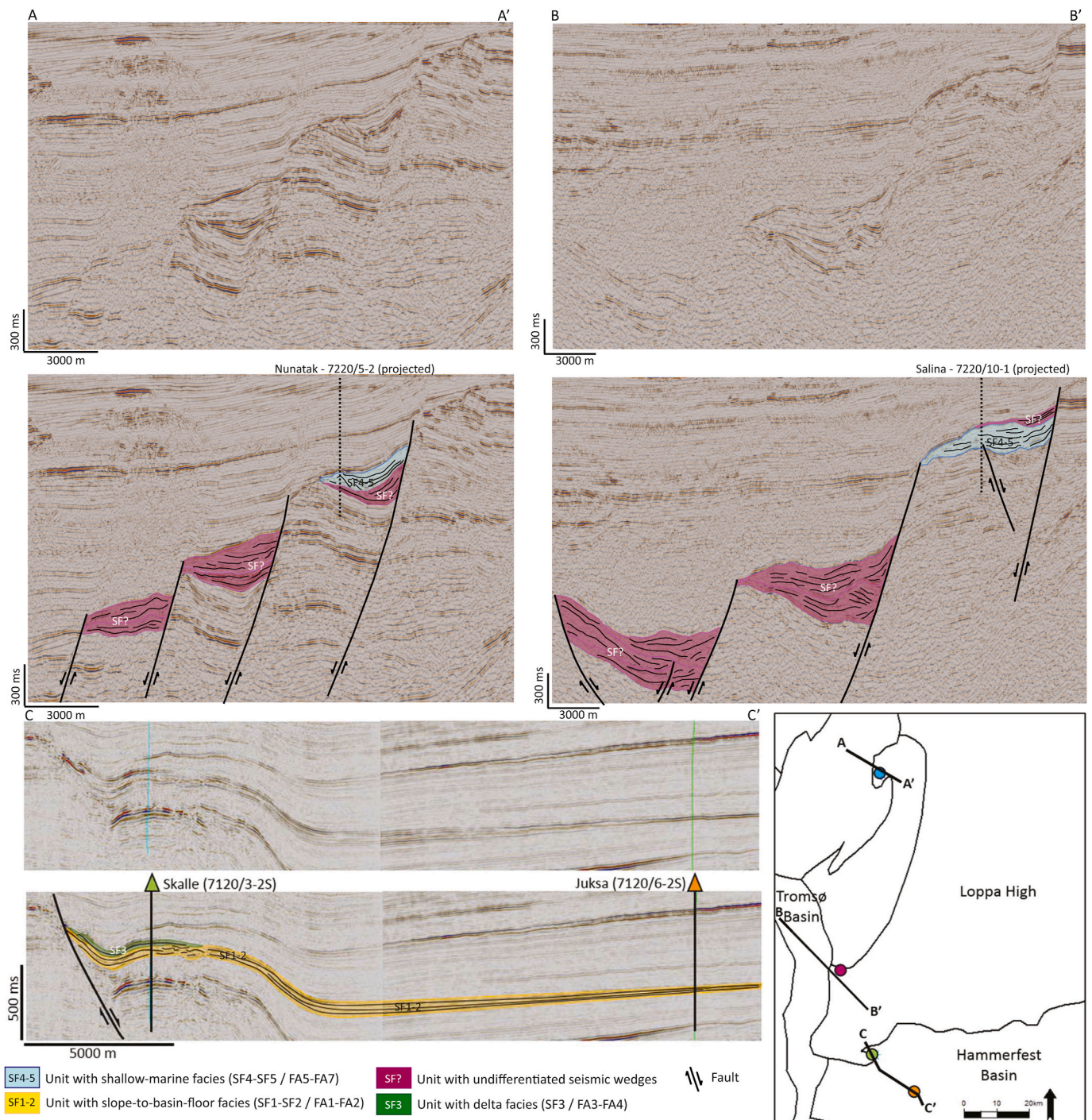
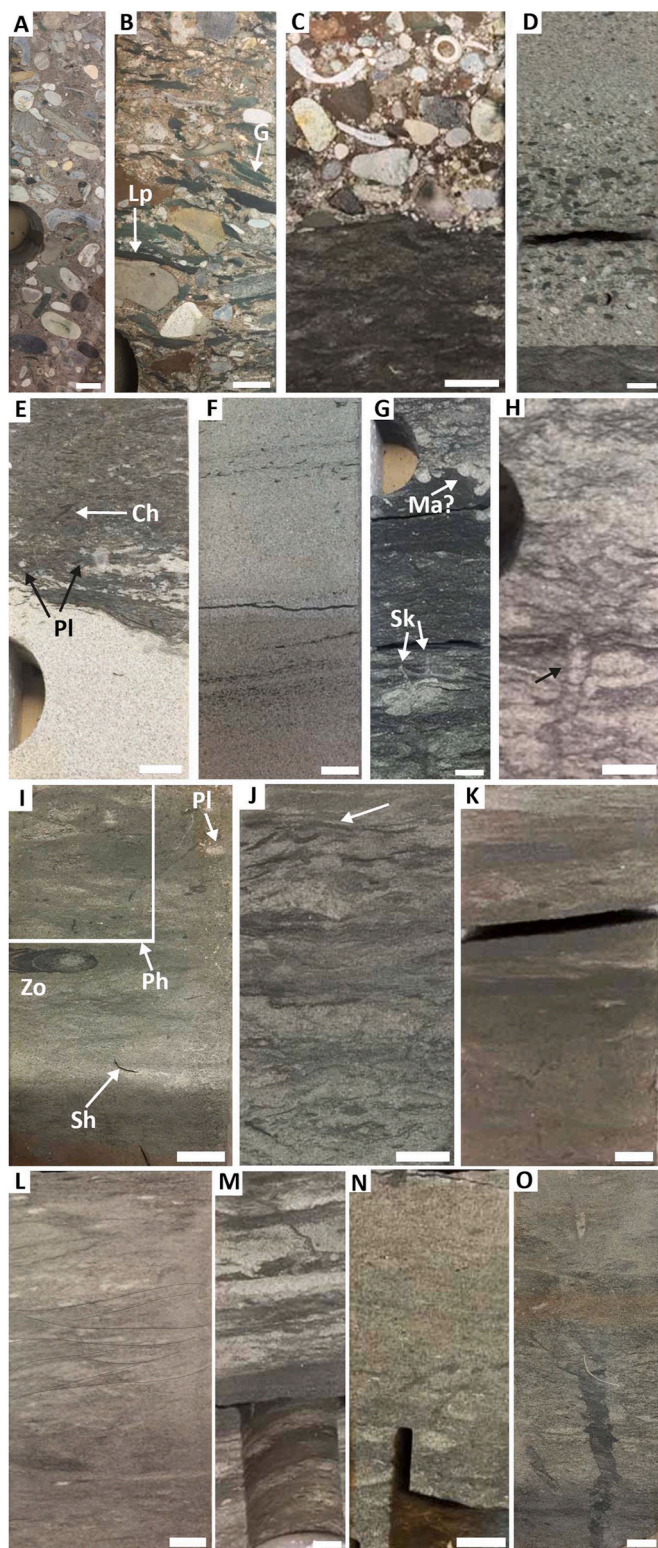


Fig. 5. Seismic lines illustrating the extension of the seismic facies into the basins for the shallow-marine (A-A', B-B') and delta and slope-to-basin-floor seismic facies (C-C'). All facies are fault-bounded towards the Loppa High. The shallow-marine facies is also offset by several normal faults (A-A', B-B'). The upper part of undifferentiated seismic wedges is truncated towards the shallow-marine facies close to the Nunatak well (7220/5-2; A-A') and the boundary between the two facies is contorted and discontinuous, indicating erosion. The well positions in lines A-A' and B-B' are projected.

that corresponds to the archetypal *Cruziana* ichnofacies, which is characteristic of shelfal environments with frequent storm activity (MacEachern and Bann, 2008). Also low-angle lamination (Figs. 3 and 6N, O) and randomly oriented shells suggest storm influence. An otherwise general low-energy environment is supported by high mud content in the sandstone. However, lower mud content than in FA5 indicates more regular wave and current action. The more proximal trace-fossil fauna than in FA5 in combination with an increase in sand content points to a shallower environment, such as an offshore transition

setting close to the fair-weather wave base.

Lower shoreface deposits (FA7; 14 m of cores in the Salina well, 7220/10-1) were suggested by Marín et al. (2018a) for the sandstone-dominated rocks in the upper cored part of the Salina well. Planar and low-angle lamina with sharp bases that include rip-up mud clasts, soft-deformed tops, and load structures were taken as indicators for frequent storm-reworking in a near-shore environment (Marín et al., 2018a).



(caption on next column)

5. Texture and composition

5.1. Texture

The grain sizes in the slope-to-basin-floor facies associations (FA1, FA2; Juksa, 7120/6-3S, and Skalle, 7120/2-3S) range from granules (ca. 2 mm) in pebbly sandstone to fine-grained to medium-grained sand (ca.

200–300 μm) in laminated and massive sandstone. Sorting is moderate in the pebbly and laminated sandstone, and mostly well sorted in the massive sandstone (Fig. 7A). Grains are subangular to subrounded. Plane grain contacts dominate except for deformed grains in the slope-channel sandstone (FA1; Fig. 7A). Grain alignment is rare. Sandstone in the deltaic facies associations (FA3, FA4; Skalle, 7120/2-3S) has more varied sorting than the slope-to-basin-floor deposits, being poorly to well sorted. It is fine to medium-grained (ca. 150–300 μm) with subangular to subrounded particles and weak grain alignment. In the poorly sorted sandstone, sand grains are loosely packed and often float in clayey matrix (Fig. 7B). The textural maturity increases upwards in the succession, and individual beds coarsen upwards. When present, point and plane contacts are most abundant (Fig. 7C). Compared to the other facies associations, the sandstone of the shallow-marine deposits (FA5 to FA7; Nunatak, 7220/5–2, and Salina, 7220/10–1) is finer-grained with very fine to fine-grained sand (ca. 100–150 μm). The sandstone has the poorest sorting, being poorly to moderately sorted, and it is dominated by subangular to subrounded grains (Fig. 7D). Bent mica grains, deformed lithoclasts, and dissolution seams also occur (Fig. 7D and E). Grain alignment is weak to lacking. Particularly the Nunatak-well sandstone (7220/5–2) contains subangular grains and detrital matrix in clusters, along lamina, as burrow fills, and as interstitial material in more coarse-grained areas. Point and plane grain contacts dominate. In the sandstone of the Salina-well reservoir (7220/10–1), subrounded grains are more common than in the Nunatak well. Sorting, roundness, and grain size also decrease from the lower shoreface (FA7) via offshore transition (FA6) to the offshore (FA5) facies associations. Plane and concavoconvex contacts prevail.

200–300 μm) in laminated and massive sandstone. Sorting is moderate in the pebbly and laminated sandstone, and mostly well sorted in the massive sandstone (Fig. 7A). Grains are subangular to subrounded. Plane grain contacts dominate except for deformed grains in the slope-channel sandstone (FA1; Fig. 7A). Grain alignment is rare.

Sandstone in the deltaic facies associations (FA3, FA4; Skalle, 7120/2-3S) has more varied sorting than the slope-to-basin-floor deposits, being poorly to well sorted. It is fine to medium-grained (ca. 150–300 μm) with subangular to subrounded particles and weak grain alignment. In the poorly sorted sandstone, sand grains are loosely packed and often float in clayey matrix (Fig. 7B). The textural maturity increases upwards in the succession, and individual beds coarsen upwards. When present, point and plane contacts are most abundant (Fig. 7C).

Compared to the other facies associations, the sandstone of the shallow-marine deposits (FA5 to FA7; Nunatak, 7220/5–2, and Salina, 7220/10–1) is finer-grained with very fine to fine-grained sand (ca. 100–150 μm). The sandstone has the poorest sorting, being poorly to moderately sorted, and it is dominated by subangular to subrounded grains (Fig. 7D). Bent mica grains, deformed lithoclasts, and dissolution seams also occur (Fig. 7D and E). Grain alignment is weak to lacking. Particularly the Nunatak-well sandstone (7220/5–2) contains subangular grains and detrital matrix in clusters, along lamina, as burrow fills, and as interstitial material in more coarse-grained areas. Point and plane grain contacts dominate. In the sandstone of the Salina-well reservoir (7220/10–1), subrounded grains are more common than in the Nunatak well. Sorting, roundness, and grain size also decrease from the lower shoreface (FA7) via offshore transition (FA6) to the offshore (FA5) facies associations. Plane and concavoconvex contacts prevail.


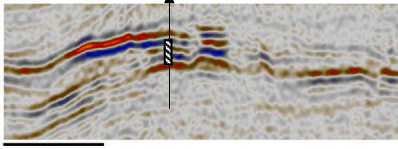
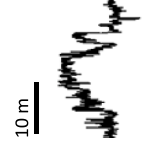

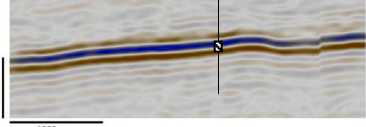
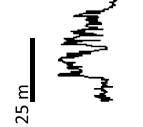

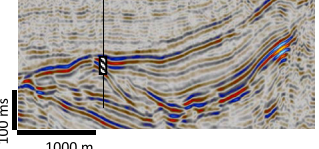


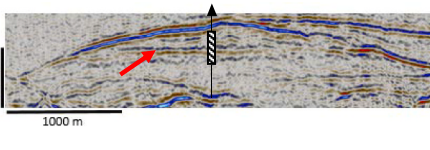
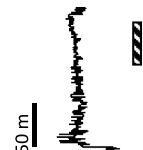
5.2. Detrital components

The sandstone ranges from subarkose to lithic subarkose and sublitharenite with mostly 75–85% quartz, 5–20% feldspar, and 5–15% lithoclasts, including pseudomatrix, in the framework (Fig. 8). The slope-to-basin-floor facies associations (FA1, FA2; Juksa, 7120/6-3S, and Skalle, 7120/2-3S) are most quartz-rich and poorest in feldspar (avg. Q₇₉F₈L₁₃ for FA1 and Q₈₁F₁₀L₉ for FA2). The slope-channel (FA1) and the deltaic facies associations (FA5 to FA7; Nunatak, 7220/5–2, and Salina, 7220/10–1; avg. Q₇₆F₁₃L₁₁) have the highest lithoclast and pseudomatrix contents (Fig. 8). Differently, sandstone of the shallow-marine facies associations (FA5 to FA7; Nunatak, 7220/5–2, and Salina, 7220/10–1) has the highest feldspar and lowest lithoclast contents (avg. Q₇₆F₁₇L₇).

For all facies associations, monocrystalline grains dominate the

Table 1

Seismic facies and gamma-ray responses for all four wells with details of seismic lines from Fig. 5. Facies associations (FA) are described in Supplementary material S3.

Well	Depositional environment	Stacking pattern	Seismic reflection	Seismic description	Gamma-ray response	Gamma-ray description
					0 200	
Skalle (7120/2-3S)	Slope-channel / delta (FA1, FA3, FA4)			Moderate to high amplitude, discontinuous reflections (upper slope to shelf-edge channel), at the top bounded by high-amplitude, continuous, sub-parallel reflections (delta).		Bow trend with decreasing-increasing values with prograding stacking pattern at bottom and top with sharp base, middle part with retrograding stacking pattern and sharp top.
Juksa (7120/6-3S)	Basin-floor fan (FA2)			High amplitude, continuous and parallel reflections bounded at the base and top by low amplitude reflections.		Highly serrated values. Fining-upwards trend.
Nunatak (7220/5-2)	Shallow-marine (FA5, FA6)			Low amplitude, continuous and sub-parallel to divergent and mounded reflections. Truncations occur locally.		Moderately high, serrated to blocky value trends with aggrading to weakly prograding stacking pattern.
Salina (7220/10-1)	Shallow-marine (FA5 to FA7)			Low amplitude, sub-continuous and sub-parallel reflections bounded by discontinuous medium (base) and high (top) reflections. Horizontal reflections in the center may represent the gas-water contact (arrow).		Low, weakly serrated to blocky values with prograding stacking pattern.

Cored intervals are marked in the seismic line and to the right of the gamma-ray curves.

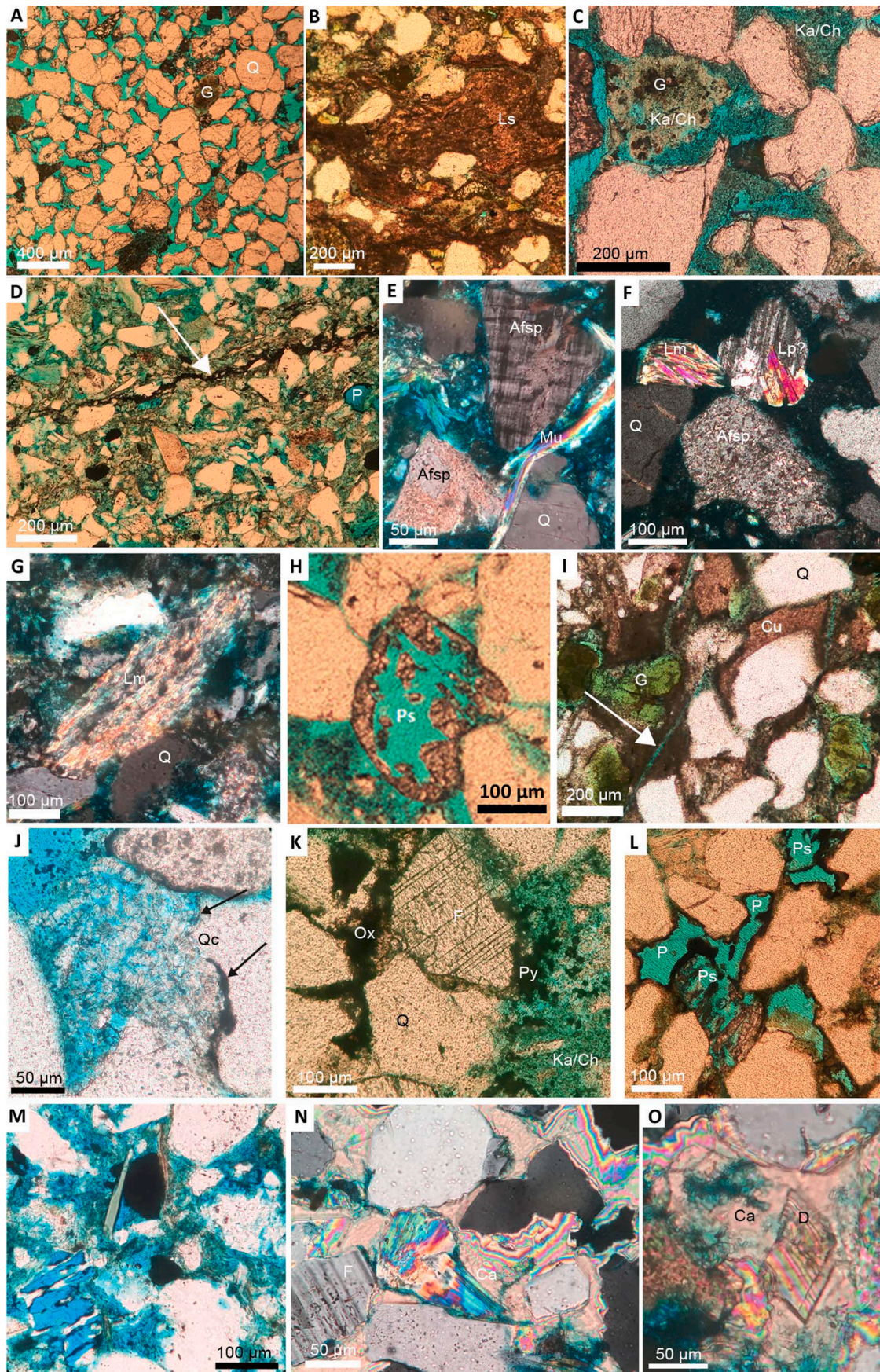
detrital quartz fraction with 50–80%, of which 40–50% are non-undulatory (Fig. 8). Both stretched grains and polygonal fabric occur among the polycrystalline grains. Chert is common with up to 13% and with the highest values for the shallow-marine deposits. Alkali feldspar dominates over plagioclase with an average ratio of 3:1 to 4:1 in all facies associations with the lowest alkali-feldspar dominance for the feldspar-poor basin-floor-fan deposits (FA2). Lithoclasts are mainly sedimentary with pelite grains being most common (Fig. 7B). Foliated metamorphic quartz-mica grains and igneous clasts (felsic volcanic and few plutonic ones with quartz + feldspar or quartz + muscovite) are less abundant, but most common in the lithoclast-rich deltaic deposits (FA3, FA4; Fig. 7F and G). In addition, rounded carbonate grains are present in the slope-to-basin-floor facies associations (FA1, FA2; Fig. 7H).

Matrix (up to 30%, but mostly lacking or < 10%) of green to brown clay commonly completely fills pore spaces or is present as clay cutanes (Fig. 7I). The highest matrix amounts occur in the deltaic deposits (avg. 12%), and the lowest in the slope-to-basin-floor facies associations (rare to lacking; avg. 1%). In the shallow-marine sandstone, it averages 9%, mainly concentrated in fine-grained bands, lamina, or in burrow linings. Pseudomatrix, included in the lithoclast fraction, is observed in all facies associations to varying extents (0–5%; avg. 2%). Also muscovite and biotite (2–11%) occur in all facies associations, but most commonly in the feldspar-rich shallow-marine deposits (FA5 to FA7; avg. 5%). There, both mica and detrital clay are less common in the Salina well than in the Nunatak well with its little abraded sand grains. Fossils – shell fragments, foraminifers, and ostracods – and ooids occur in all facies associations with of up to 6%, and are particularly common in the slope-to-basin-floor deposits (FA1, FA2). In the shallow-marine sandstone (FA5 to FA7), fossils predominantly are concentrated in storm-event beds. Glauconite is particularly common in the lithoclast-rich and pseudomatrix-rich deltaic (FA3, FA4; avg. 6%; Fig. 7C, H) and slope-channel deposits (FA1; avg. 3%).

5.3. Diagenetic minerals

Diagenetic minerals constitute 5–30% of the rock volume and include clay minerals, carbonate, quartz, and more rarely feldspar, pyrite, hematite and anhydrite. Microscope observations and XRD data suggest that authigenic clay minerals (<20%) are kaolinite, chlorite, illite, and glauconite. XRD patterns also have broad peaks at ca. 20° and 35° 2θ (ca. 4.4 Å and 2.6 Å in lattice distance), indicating disordered/mixed-layer clay (Brindley and Brown, 1980; Moore and Reynolds, 1997). Quartz cement (2–8%) is present in all facies associations. It occurs as thin overgrowths, or locally as outgrowths, around quartz grains (Fig. 7J). Carbonate cement, mostly calcite, generally composes <1% with the exception of the slope-to-basin-floor facies associations (FA1, FA2; up to 3%); few sandstone samples are strongly carbonate-cemented (up to 25%). The other cement minerals occur in minor amounts in all facies associations (<7%). Pyrite is present as fine, euhedral to subhedral intergranular crystals and mixed with authigenic clay minerals (Fig. 7K). Fe oxide often has stained grains, matrix and other cement, but is also occasionally enclosed by quartz and authigenic clay minerals (Fig. 7K). When together, pyrite is engulfed or replaced by Fe oxide. Rare feldspar cement occurs as partly dissolved rims around feldspar grains engulfed by authigenic clay minerals. Traces of hydrocarbon are present in all facies, staining or engulfing clay-mineral rims, around dissolved grains, or filling pores (Fig. 7L).

With some differences, the slope-to-basin-floor (FA1, FA2; Juksa, 7120/6-3S, and Skalle, 7120/2-3S) and deltaic facies associations (FA3, FA4; Skalle, 7120/2-3S) include similar diagenetic features. The slope-channel (FA1), basin-floor-fan (FA2), and deltaic (FA3, FA4) sandstone has authigenic clay-mineral contents of 1–10%, 8–19%, and 2–18%, respectively. The clay-mineral content decreases as detrital clay matrix increases in the deltaic deposits, thus giving a nearly constant amount of total clay, although a decrease is observed upwards in the succession. The slope-to-basin-floor and deltaic facies associations have



(caption on next page)

Fig. 7. Microphotographs in plane-polarised light (except E, F, G, N, O: double-polarised light). **A.** Well sorted massive sandstone (facies F5) with high porosity and point and plane contacts of facies association FA1 (slope channel), well Skalle (7120/2-3S), 1635.8 m. **B.** Deformed pelitic lithoclasts as pseudomatrix, FA4 (delta front), well Skalle, 1600.1 m. **C.** Glauconitic sandstone (F10) with kaolinite and chlorite replacing altered glauconite, and point and plane contacts, FA4 (delta front), well Skalle, 1587.1 m. **D.** Poorly sorted sandstone with subangular grains and a dissolution seam (arrow), FA6 (offshore transition), well Nunatak (7220/5-2), 1287.5 m. **E.** Bent muscovite grain next to sericitized alkali feldspar, FA5 (offshore), well Nunatak, 1306.3 m. **F.** Probable plutonic lithoclast above partly sericitized alkali feldspar, FA2 (basin-floor fan), well Juksa (7120/6-3S), 1989.3 m. **G.** Metasedimentary lithoclast with quartz and mica, FA6 (offshore transition), well Nunatak, 1280.7 m. **H.** Partly dissolved carbonate fragment with intragranular porosity, FA1 (slope channel) well Skalle, 1635.8 m. **I.** Glauconitic sandstone with thick clay cutanes and a shrinkage fracture (arrow), FA3 (prodelta/delta slope), well Skalle, 1602.1 m. **J.** Massive sandstone (F5) with kaolinite booklets and quartz overgrowths (arrows), FA1 (slope channel), well Skalle, 1635.8 m. **K.** Fe-oxide-replaced pyrite that stains also authigenic clay minerals. A kaolinite-chlorite mix fills the pore to the right, FA2 (basin-floor fan), well Juksa, 1984.4 m. **L.** Primary intergranular pores and intragranular secondary pores surrounded by hydrocarbon-stained chlorite rims, FA2 (basin-floor fan), well Juksa, 1975.7 m. **M.** Pore-filling meshwork of illite and chlorite and a dissolved feldspar grain (lower left), FA5 (offshore), well Nunatak, 1314.5 m. **N.** Only weakly compacted sandstone due to poikilotopic calcite cement, FA5 (offshore), well Nunatak, 1306.5 m. **O.** Dolomite rhomb surrounded by calcite cement, FA5 (offshore), well Nunatak, 1306.5 m. Afsp = alkali feldspar, Ch = chlorite, Ca = calcite, Cu = clay-mineral cutane, D = dolomite, G = glauconite, Ka = kaolinite, Lm = metamorphic lithoclast, Lp = plutonic lithoclast, Ls = sedimentary lithoclast, Mu = muscovite, Ox = Fe oxide, P = pore, Ps = secondary porosity, Py = pyrite, Q = quartz.

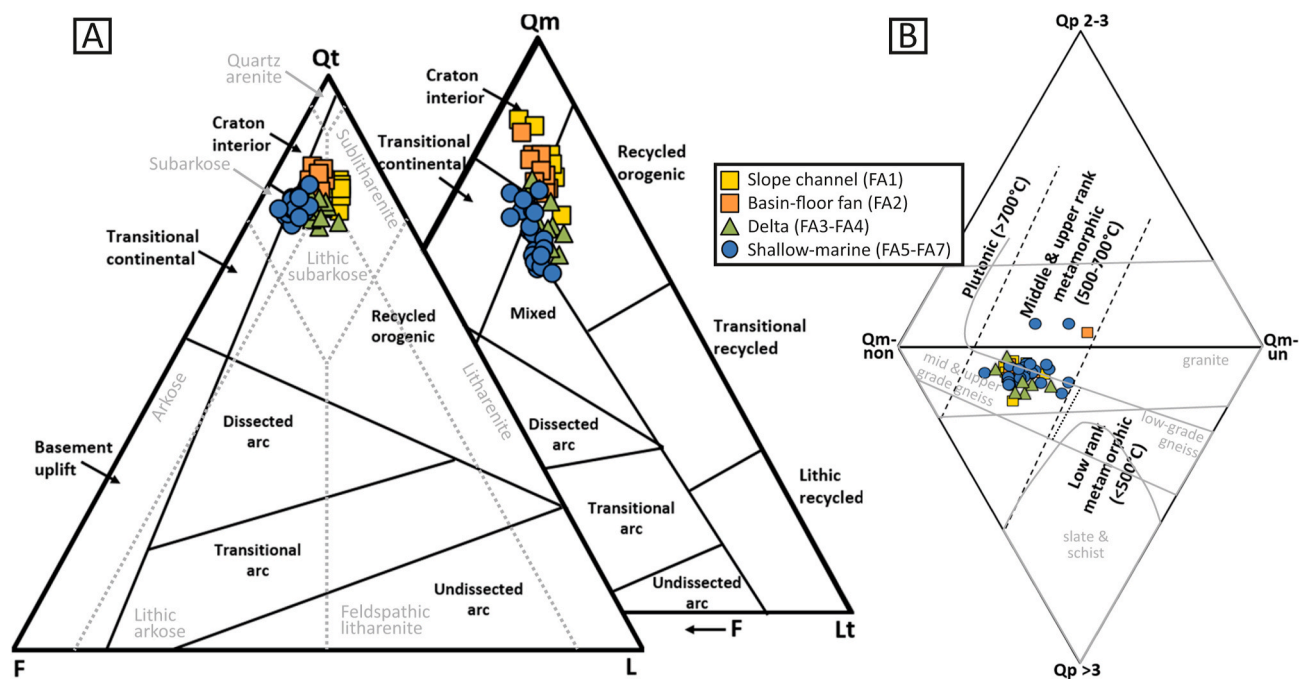


Fig. 8. **A.** Framework petrographic composition with discrimination fields for sandstone classification from McBride (1963; grey) and for provenance from Dickinson et al. (1983; black). **B.** Quartz-grain characteristics with discrimination fields for provenance from Basu et al. (1975; black) and Tortosa et al. (1991; grey). Q = quartz, Qm = monocrystalline Q, Qm-non = non-undulatory Qm (<5°), Qm-un = undulatory Qm (>5°), Qp = polycrystalline Q, Qp 2-3 = Qp with 2-3 crystals, Qp > 3 = Qp with >3 crystals, Qt = total Q (including Qp and chert), F = feldspar, L = lithoclasts (including pseudomatrix), Lt = total L (including Qp and chert).

higher kaolinite and chlorite contents than the shallow-marine deposits (FA5 to FA7). The chlorite occurs as pore-lining coats around detrital and dissolved grains (with the thickest and most continuous coats in massive sandstone of the basin-floor-fan deposits) or as ridges between grains. Kaolinite mixed with chlorite occurs in primary and secondary pores and as alteration products of lithoclasts and glauconite (Fig. 7J and K). Particularly in the deltaic sandstone (FA3, FA4), the kaolinite-chlorite mix occasionally completely fills pores. In the slope-to-basin-floor deposits (FA1, FA2), thick and blocky kaolin polytypes, possibly dickite (not confirmed by XRD), are identified (Fig. 7J) and illite only occurs in few sericitized alkali-feldspar grains. In the deltaic facies associations (FA3, FA4), illite instead is mixed with detrital matrix. Broad XRD peaks at ca. 10 Å in matrix-rich deltaic sandstone also may indicate illite/smectite layers (Brindley and Brown, 1980; Moore and Reynolds, 1997). The carbonate cement in the sandstone of the slope-to-basin-floor and deltaic deposits is grain-rimming, often with signs of secondary dissolution. In the slope-to-basin-floor sandstone (FA1, FA2) it has been followed by crystallization of rhomb-shaped siderite surrounded by iron staining. Its optical properties and a high Fe content suggests Fe-rich siderite, although the XRD data indicates rhodochrosite. Siderite

formation was followed by pore-filling finely crystalline calcite. Where together, carbonate cement covers or replaces authigenic clay coats, and is engulfed or replaced by pore-filling clay in both the slope-to-basin-floor and deltaic deposits. Authigenic quartz and grain-coating chlorite correlate negatively. Quartz cement is discontinuous to lacking where thick clay coats continuously cover quartz grains and in sandstone that is rich in carbonate cement. Where occurring together, most quartz cement covers or encloses pore-filling or grain-replacing kaolinite/chlorite, and thus postdates chlorite coats and carbonate cement, but authigenic quartz is occasionally engulfed by carbonate and grain-rimming clay cement. Pyrite is common in the basin-floor-fan sandstone (FA2), and most rare in the sandstone of the deltaic facies associations (FA3, FA4).

The sandstone of the shallow-marine facies associations (FA5 to FA7; Nunatak, 7220/5-2, and Salina, 7220/10-1) has an authigenic clay-mineral content of 5–18% with the lowest values for the Salina well, similar to the trend for detrital clay. Different to the other facies associations, abundant illite is mixed with chlorite. The illite-chlorite mix is most common as a completely pore-filling meshwork (Fig. 7M) but also occurs as thin, discontinuous grain-rimming plates or fibers or as

replacement for kaolinite, feldspar or detrital mica grains. Kaolinite occasionally is present in oversized pores as replacement for feldspar and mica grains. Most carbonate cement is poikilitic, pore-filling and occurs in clusters or has replaced feldspar (Fig. 7N). It is often in contact with grains or was preceded by thin quartz rims. Clay-mineral cement is rare in calcite-rich areas, but where observed together, calcite is engulfed by it. Trace amounts of rare rhombohedral dolomite crystals that either engulf or are replaced by calcite also are present (Fig. 7O). Quartz cement is most common (4–8%) in the shallow-marine sandstone. Different to the other facies associations, no correlation exists between the amount of authigenic quartz and clay minerals. However, quartz-cement rims are commonly thinner or absent where clusters of calcite are present, and it is sometimes preceded by kaolinite and illite rims. Anhydrite is observed in trace amounts. Also different to the other facies associations, pore-filling hydrocarbon is preceded by poikilitic calcite, but is engulfed by a meshwork of authigenic clay minerals. Pyrite is common.

5.4. Porosity

Thin-section porosity varies from 1 to 20% (Fig. 9), including 1–8% secondary porosity (avg. 4%). The intergranular volume (intergranular porosity and cement) is <25% for all facies. The overall porosity is particularly high for matrix-poor sandstone and sandstone with little carbonate cement (Fig. 9). It is lower in sandstone with abundant mica and feldspar grains, as well as in pseudomatrix-rich sandstone and sandstone with thick authigenic chlorite coats. The pores are less interconnected in poorly sorted sandstone with abundant clay matrix than in better sorted sandstone. The intragranular pores usually are isolated from the rest of the pore system.

Primary porosity dominates both in slope-to-basin-floor (FA1, FA2; Juksa, 7120/6-3S, and Skalle, 7120/2-3S) and deltaic facies associations (FA3, FA4; Skalle, 7120/2-3S), and these have total porosity contents of on average 13% and 8%, respectively. The porosity is particularly high in massive sandstone of the basin-floor-fan deposits (FA2; 12–19%) and deltaic sandstone (FA3, FA4) with little detrital clay matrix. In the slope-to-basin-floor sandstone (FA1, FA2), the amount of porosity seems to be little affected by the presence of mica and feldspar (Fig. 9). Intragranular secondary pores both in the slope-to-basin and deltaic deposits often occur in partly dissolved feldspar and more rarely lithoclasts and detrital quartz grains. They are commonly filled with the kaolinite-chlorite mix

and are engulfed by chlorite coats or detrital clay rims (Fig. 7L). Pseudomorphic pores and partially leached quartz and carbonate cement are also present as intergranular secondary porosity in the slope-to-basin-floor sandstone and shrinkage porosity is observed in deltaic sandstone with abundant clay matrix (Fig. 7I).

The sandstone of the shallow-marine facies associations (FA5 to FA7; Nunatak, 7220/5–2, and Salina, 7220/10–1) has the lowest porosity with an average of 8% for the Nunatak well and 5% for the Salina well; secondary porosity dominates. The porosity is highest in sand-rich layers and lowest in mud-rich lamina or burrow linings and decreases with the grain size from lower shoreface (FA7) to offshore deposits (FA5). The intergranular pores are poorly connected due to the separation of porous sandstone layers by low-porosity lamina. The amount of porosity and feldspar + mica correlate positively (Fig. 9). Also partly different to the other facies associations, the secondary porosity is caused by dissolution of feldspar and mica grains, and more rarely of quartz cement (Fig. 7M). Furthermore, the secondary pores are often filled with kaolinite, illite and chlorite. Primary pores are filled with quartz outgrowths, illite, chlorite or poikilitic calcite.

5.5. Geochemical composition

Sandstone from all investigated facies associations has SiO₂ concentrations of 70–90%, except for anomalously CaO-rich sandstone. The SiO₂ correlates with the quartz content. Anti-correlative, reservoir sandstone contains 2–12% Al₂O₃. Other major oxides correlate with Al₂O₃. CaO generally is <1%. Sandstone with higher CaO concentrations also has anomalously high MnO and loss-of-ignition values. Na₂O/K₂O is low, mostly <1 (exception: > 1 for the basin-floor-fan sandstone, FA2, with the lowest alkali feldspar-plagioclase ratio) and the Chemical Index of Alteration is 62–72. The basin-floor-fan sandstone (FA2) follows the ideal weathering trend as defined by Fedo et al. (1995). Sandstone of the other facies associations is slightly enriched in K, thus deviating from the ideal weathering trend.

Zr/Sc and Th/Sc are 10–80 and 0.4–1.6, respectively (Fig. 10). Ti/Zr and La/Sc are 8–16 and 1.7–5.5, respectively (Fig. 10). The provenance-indicative Zr/Sc, Th/Sc, and La/Sc are the highest for the mineralogically mature basin-floor-fan sandstone (Fig. 10; FA2; avg, 48, 1.6, and 4.3, respectively) and the lowest for the matrix-rich delta facies associations (FA3 and FA4; avg, 19, 0.5, and 2.4, respectively).

In general, REE concentrations are lower than for post-Archean

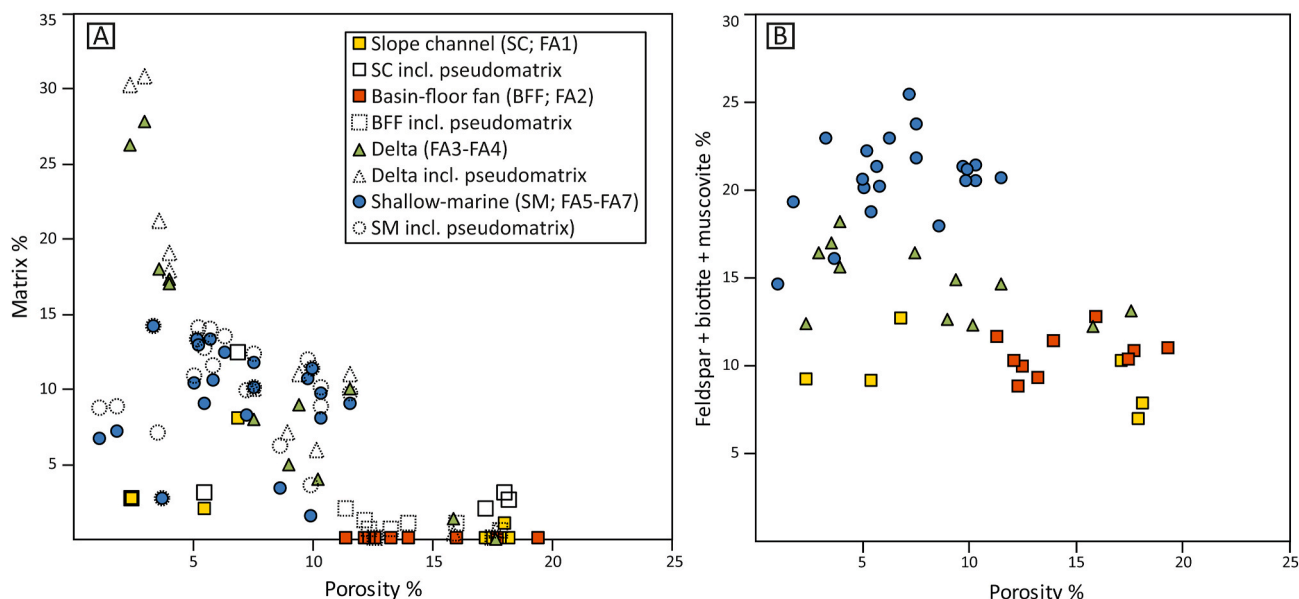


Fig. 9. A. Porosity vs. matrix and pseudomatrix. B. Porosity vs. feldspar + mica.

Average Australian Shale (Taylor and McLennan, 1985), but with a similar enrichment of light over heavy REEs. This is reflected by La/Yb ratios of 7–11. Eu_N/Eu^* is mostly 0.7–0.8. The sandstone of the slope-to-basin-floor facies associations (FA1, FA2) is particularly depleted in REEs due to quartz dilution.

6. Discussion

6.1. Provenance and depositional reservoir-quality factors

The partly abundant detrital mica indicates that the Loppa High is the most probable detrital source area (Fig. 11) as mica only survives a short distance in the transport system with the sand fraction (e.g., Doyle et al., 1983; Qin et al., 2018). A Loppa-High source is also supported by the wedge-shaped seismic reflectors thickening towards the high. The framework-compositional similarities between sandstone of all studied facies associations, independent of well location, indicate that the catchment areas on the Loppa High were of rather similar lithology. Thereby, the high quartz abundance suggests a recycled orogenic provenance (Fig. 8; Dickinson et al., 1983). Similarly, the enrichment of incompatible over compatible elements such as Th/Sc and La/Sc and the low Eu_N/Eu^* are typical for detritus from old continental crust (Bhatia and Crook, 1986; McLennan et al., 1990, 1993). The metamorphic lithoclasts and the dominance of monocrystalline quartz with non-undulatory extinction suggests transport ultimately from middle to upper rank metamorphic quartz-prone source rocks (Fig. 8; Basu et al., 1975; Tortosa et al., 1991). However, the abundant sedimentary lithoclasts indicate transport from sedimentary rocks that capped the crystalline Loppa-High basement. Also the occasional quartz overgrowths preceding clay-mineral introduction indicate that some quartz cement is inherited from an earlier sedimentary cycle, indicating that these grains were recycled. Indeed, the basement is covered with Carboniferous, Permian, and Triassic strata (Indrevær et al., 2017). Thus, recycled Triassic, or eroded Jurassic, detritus is the most likely dominating source for the Early Cretaceous deposits, as also was suggested by Sattar et al. (2017) based on seismic interpretations. Also other Early Cretaceous basins in the southwestern Barents Sea are interpreted to have been fed by recycled Triassic detritus from locally uplifted highs (Gabrielsen et al., 1990; Faleide et al., 1993; Seldal, 2005; Worsley, 2008; Marín et al., 2018a). Triassic sandstone in the Western Barents Sea is reported to be subarkosic to arkosic, containing more potassium feldspar than plagioclase and abundant schist lithoclasts (Mørk, 1999), thus being in accordance with recycling into the Lower Cretaceous deposits of this study.

The enrichment of feldspar in the shallow-marine facies associations of the Salina (7220/10–1) and Nunatak (7220/5–2) wells west of the

Loppa High may suggest that the siliciclastic source-rock lithology was slightly different in the west than in the south where the deltaic and slope-to-basin-floor deposits of the Skalle (7120/2-3S) and Juksa wells (7120/6-3S) occur. Also the lower mica and higher lithoclast contents of the sandstone in the south indicate minor variations in source-rock lithology. In addition, the chert and rare carbonate fragments suggest that carbonate-rich strata were available for erosion on the Loppa High. The higher abundance of chert and lower abundance of pelitic lithoclasts for the shallow-marine than the deltaic and slope-to-basin-floor deposits indicate that carbonate detritus was more available in the west than in the south. The presence of carbonate units is confirmed as Carboniferous and Permian carbonate strata have been penetrated on the Loppa High (e.g., Stemmerik et al., 1999; Sayago et al., 2012). As Aptian-Albian tilting caused a steeper western than eastern flank on the Loppa High (Marín et al., 2018a), the Triassic cover in the west may preferentially have been eroded in deeply incised valleys. Such erosional topography has been identified for the Early Cretaceous margin of the Loppa high (Sattar et al., 2017; Marín et al., 2018b).

Variations in tectonic activity seem to have had a limited effect on sandstone mineralogy because of the clearly higher texturally maturity but only slightly higher mineralogical maturity of the shallow-marine Albian sandstone of the Salina well (7220/10–1) than the Aptian deposits of the Nunatak well (7220/5–2). As the Albian was a quieter tectonic phase than the Aptian (cf. Kairanov et al., 2019), a mineralogical distinction between these two reservoirs could have been expected. Differently, in the south reworking resulted in enrichment of quartz and related immobile trace elements for the basin-floor-fan sandstone only, as indicated by the slightly elevated incompatible to compatible element ratios, Zr/Sc, compositional and textural maturities (cf. Correns, 1978; McLennan et al., 1993).

The rather similar framework-petrographic and geochemical compositions for all studied facies associations indicate that the provenance was only a minor factor controlling the resulting reservoir quality. Instead, most variations in reservoir-quality properties are probably related to the depositional conditions. The texture and diagenetic features indicate that the amount of porosity was more affected by the amount of matrix than by grain size in the framework (which is strongly linked to sorting, cf. Beard and Weyl, 1973) except for the trends of decreasing grain size and porosity from lower shoreface to offshore sandstone. This is illustrated by the matrix-poor slope-to-basin-floor sandstone with the best sorting and highest porosity. Dewatering structures in the slope-to-basin-floor facies associations may have removed or concentrated detrital clay from the sediment and thus enhanced the sorting. Similarly, dewatering has contributed to well-sorted Cretaceous-Paleogene deep-marine sandstone in the Norwegian Sea (Lien et al., 2006).

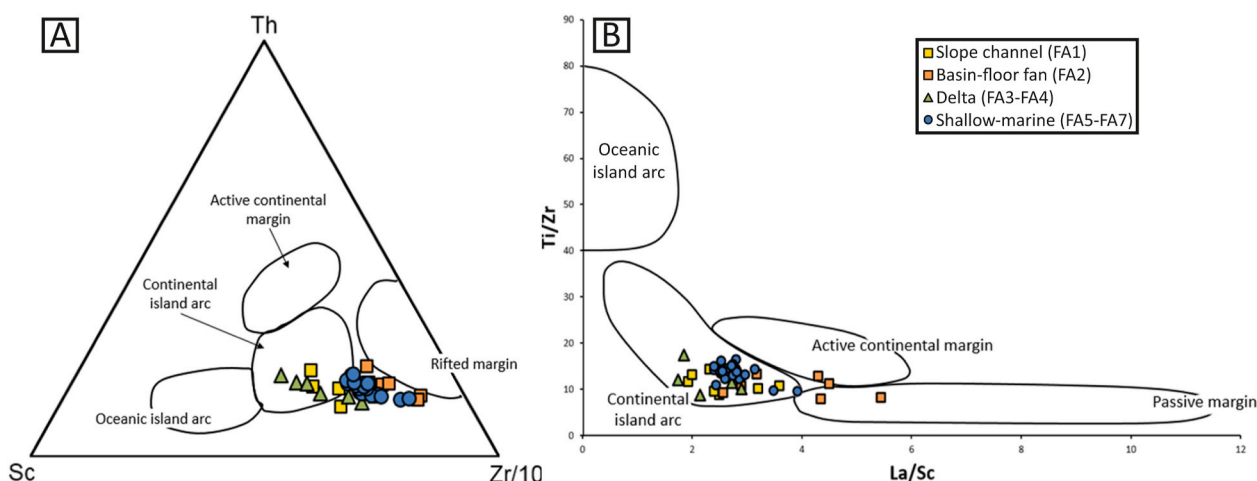


Fig. 10. Trace element compositions with discrimination fields for tectonic settings from Bhatia and Crook (1986). A. Th vs. Sc vs. Zr. B. La/Sc vs. Ti/Zr.

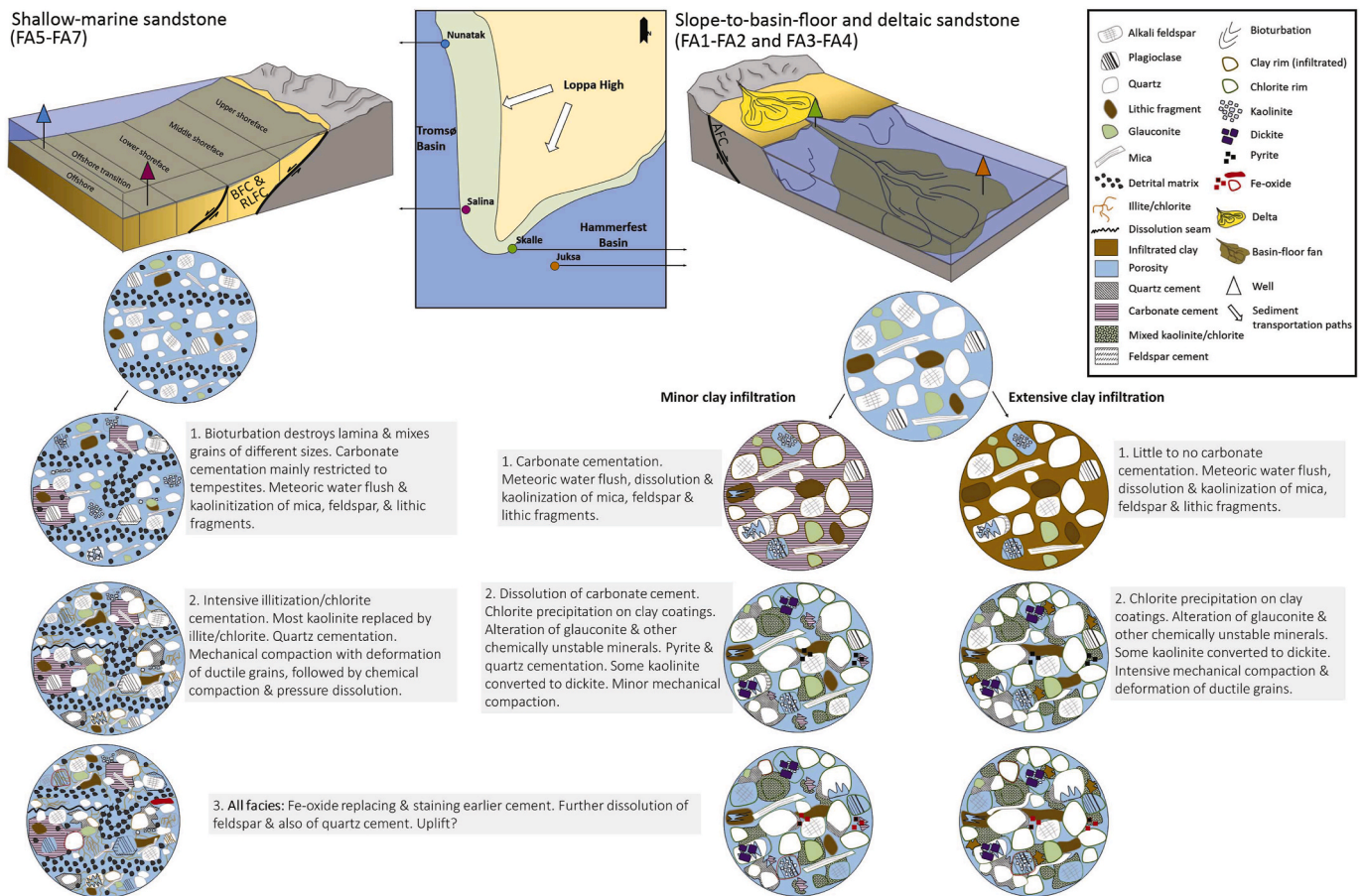


Fig. 11. Diagenetic processes and related reservoir-quality-evolution pathways. Note that the (Aptian) Nunatak and (Albian) Salina deposits are diachronous. The white arrows in the map roughly illustrate the sediment-transportation paths. AFC = Asterias Fault Complex, BFC = Bjørnøyrenna Fault Complex, RLFC = Ringvassøy-Loppa Fault Complex.

It is likely that both the matrix-rich sandstone with few interconnected pores in the deltaic and shallow-marine facies associations and the fine-grained lamina in the shallow-marine sandstone act as barriers for fluid flow (cf. [Ketzer and Morad, 2006](#); [Morad et al., 2010](#)). Also partly abundant mechanically unstable lithic grains may have led to rapid decline in both porosity and permeability during mechanical compaction ([Fig. 11](#)). Thus, the permeability is assumed to be lowest in the shallow-marine sandstone. Similarly, the lack of correlation between porosity and mica + feldspar for the basin-floor-fan sandstone can be due to the sparse mica and feldspar grains, lack of illitized feldspar, and the high primary-to-secondary porosity ratio. However, also other diagenetic processes than compaction, such as pressure solution and illitization of mica and feldspar, may have reduced the reservoir quality ([Fig. 11](#)).

6.2. Diagenetic processes influencing reservoir quality

The major diagenetic porosity-reducing factors in this study are bioturbation, compaction, clay infiltration, authigenic clay-mineral precipitation, and quartz and carbonate cementation ([Fig. 12](#)). The low intergranular volumes and the more common intergranular cement than intergranular porosity indicate that compaction has dominated over cementation in reducing porosity for all facies associations (cf. [Ehrenberg, 1989](#)).

Porosity-enhancing factors include dissolution and the precipitation of clay coats around detrital grains. Post-depositional modifications of the reservoir quality mainly were eodiagenetic to mesodiagenetic, but also telodiagenetic due to uplift ([Figs. 11 and 12](#)). The low abundance of

hydrocarbon and the later growth of quartz and illite suggest that the hydrocarbon emplacement did not cause diagenetic variation for the different facies associations (cf. [Ehrenberg and Nadeau, 1989](#); [Bloch et al., 2002](#)).

The overall weathering trend and the observed kaolinite for the basin-floor-fan sandstone indicates conversion of feldspar to kaolinite (cf. [Fedo et al., 1995](#)). Some depletion of the mobile elements Ca, Na, and K also may have been caused by alteration during reworking and related processes. The kaolinite-illite mix in the shallow-marine facies associations is in agreement with K addition due to conversion of kaolinite to illite (cf. [Fedo et al., 1995](#)). Most other K addition probably is attributed to the abundant glauconite in the deltaic and slope-channel facies associations (cf. [Velde, 2003](#)).

6.2.1. Early clay infiltration in the slope-to-basin-floor (FA1, FA2) and deltaic deposits (FA3, FA4)

The similar authigenic composition and texture for the sandstone in the slope-to-basin-floor and deltaic facies associations indicate a common paragenetic sequence ([Fig. 12](#)). The massive, pore-bridging, and grain-covering clay matrix indicates infiltrated clay that leads to enrichment of clay particles but leaves the initial sand texture unaffected ([Walker, 1976](#); [Matlack et al., 1989](#); [Moraes and De Ros, 1990; 1992](#)). The authigenic clay-mineral precipitation may have been controlled by the amount and type of infiltrated clay as it acted as nucleation sites on grain surfaces and in pores for the authigenic chlorite and illite-kaolinite mix. Therefore, we assume that both detrital and authigenic clay rims were introduced before most compaction took place ([Figs. 11 and 12](#)). Different to the other environments, it is likely

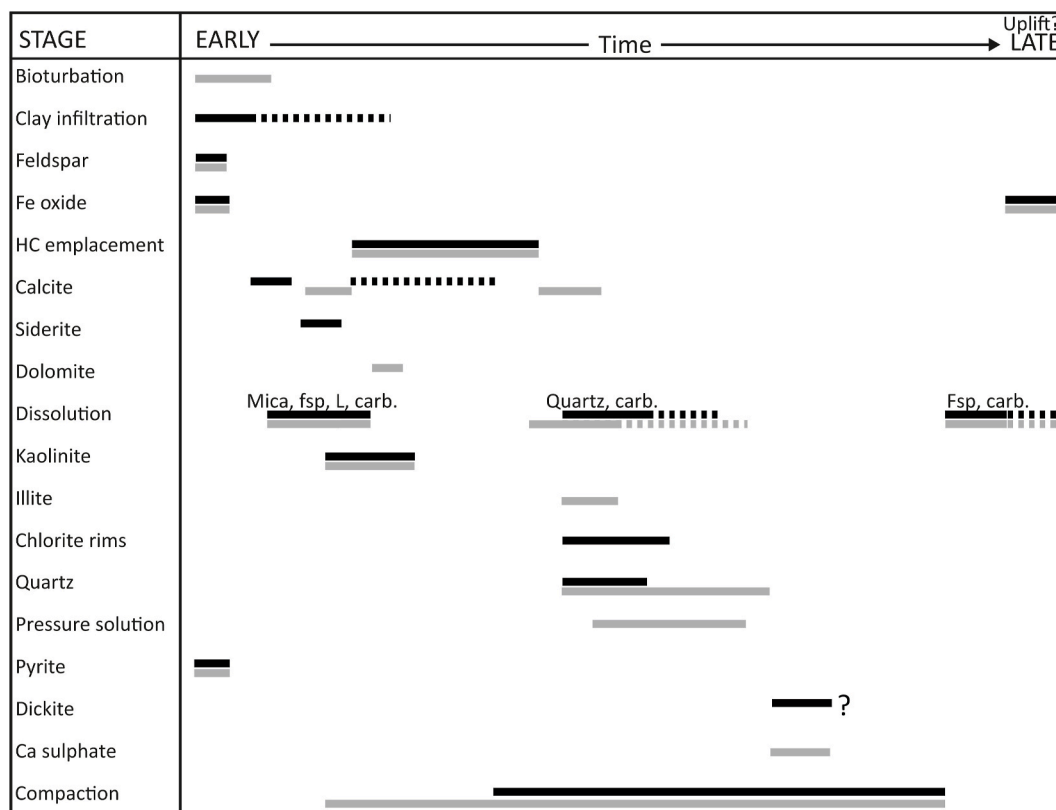


Fig. 12. Paragenetic sequences for slope-to-basin-floor and deltaic (black) and shallow-marine facies associations (grey). The observed calcium sulphate is anhydrite, but a gypsum precursor is likely. Dissolved components are stated over the corresponding dissolution phase. Carb. = carbonate, fsp = feldspar, HC = hydrocarbon, L = lithoclasts.

that detrital grains in the basin-floor-fan deposits were covered by cutanes before mass transportation because it is an atypical environment for clay infiltration. Alternatively, the clay rims were emplaced by dewatering processes (cf. Houseknecht and Ross, 1992).

The infiltrated clay and related authigenic products affected the reservoir quality in several aspects: (1) The general low content of quartz cement and the inverse relationship with clay coats suggest that early introduction of clay minerals inhibited quartz growth and preserved primary porosity (Fig. 11; cf. Ehrenberg, 1993; Pittman et al., 2010). (2) The clay minerals caused little carbonate precipitation as carbonate cement is rare in sandstone with much clay. However, where present, traces of dissolved carbonate cement suggest that it both prevented mechanical compaction and enhanced porosity during later dissolution (Fig. 11). Finally, (3) ductile grains in clay-rich sandstone are deformed, so most mechanical compaction occurred after carbonate precipitation. In conclusion, moderate clay infiltration, enough to cover grain surfaces and to prevent quartz growth, combined with moderate carbonate cementation and later dissolution has been most beneficial to preserve the original reservoir quality (Fig. 11).

6.2.2. Other diagenetic processes in the slope-to-basin-floor (FA1, FA2) and deltaic deposits (FA3, FA4)

It is probable that much of the glauconite derived from reworked sediment as it rather forms in marine environments of lower sedimentation rates than the studied parts of the deltaic and slope-to-basin floor systems (Velde, 2003). Pyrite formed at an initial diagenetic stage due to bacterial sulphate reduction just below the sea floor (Raiswell, 1987). It was followed by carbonate precipitation, whereby the presence of both carbonate and chert grains make intraformational bioclasts and carbonate grains a plausible main carbonate source (cf. Milliken et al., 1998; Morad et al., 2010). The carbonate, feldspar rims, and kaolinite also indicate an early phase of carbonate and feldspar dissolution with

corresponding precipitation, post-dating the clay infiltration (Fig. 11). The dissolution may have been attributed to meteoric water flow as a result of relative sea-level fall and progradation of the depositional systems in a near-coastal setting (cf. Morad et al., 2010) caused by uplift of the Loppa High (Fig. 11; Marín et al., 2018a). Alternatively, it was controlled by overpressure from high sedimentation and burial rates (Yang et al., 2009). Dissolution features also in the distal slope-to-basin-floor deposits may indicate that meteoric water was substantial enough to reach the deep basin (cf. Mansurbeg et al., 2006, 2020; Prochnow et al., 2006). The thin Fe-oxide rims reveal that its precipitation sometimes preceded quartz overgrowth.

The majority of quartz cementation probably occurred during mesodiagenesis, coeval with clay-mineral precipitation on infiltrated clay and from glauconite (Figs. 11 and 12). Late clay-mineral precipitation and alteration of chemically unstable minerals imply a second dissolution phase, possibly due to minor chemical compaction as indicated by the dominance of point and plane contacts and the relatively low content of quartz cement (Figs. 11 and 12). The minor compaction is probably due to the presence of grain-rimming clay minerals (e.g., Engelhardt, 1960; Gaupp and Okkerman, 2011).

The blocky dickite may have formed from vermicular, booklet-like kaolinite, generally a late diagenetic process that starts at moderate to deep burial depths (>3000 m; Beaufort et al., 1998). This is in line with estimated maximum burial depths of approximately 3 km for the slope-to-basin-floor and deltaic reservoirs (Baig et al., 2016; Ktenas et al., 2019). Furthermore, the pyrite-replacing Fe oxide suggests oxidizing conditions during telodiagenesis due to renewed introduction of meteoric water. The late Fe oxide is in line with Cenozoic inversion, regional uplift to the present-day reservoir depths of 1570–1990 m and erosion of large parts of the Barents Shelf (cf. Doré et al., 1999; Henriksen et al., 2011).

6.2.3. Diagenetic processes in the shallow-marine facies associations (FA5 to FA7)

The paragenetic sequence for the shallow-marine facies associations is similar to the other facies associations in respect to (1) feldspar and carbonate cement predating most other cement types (Figs. 11 and 12), (2) the carbonate source likely being carbonate bioclasts, explaining the clustered appearance of most carbonate cement, (3) early dissolution and kaolinitization of feldspar, lithoclasts, and mica that probably is due to meteoric water flow, and (4) eodiagenetic mechanical compaction that similarly deformed lithoclasts and bent mica grains (Fig. 12). Different to the other facies associations, early bioturbation that partly destroyed lamina and mixed grains of different sizes caused unsorting and decrease in both porosity and permeability (Fig. 11). Also the clustered and sporadic distribution of carbonate cement suggests that the cement rather increased the reservoir heterogeneity than inhibited and impacted compaction and subsequent diagenetic phases. The early calcite precipitation was followed by dolomitization and a second phase of calcite that replaced dolomite (Fig. 12). Furthermore, the frequent concavoconvex grain contacts and the illite-replaced kaolinite and feldspar indicate that the authigenic quartz is tied to chemical compaction and illite precipitation. Illite formation follows the reaction of alkali feldspar and kaolinite at temperatures above 70 °C, and is most pervasive at 130–140 °C (ca. 3.7 km; cf. Ehrenberg and Nadeau, 1989; Worden and Morad, 2003). This reaction thus suggests a second stage of dissolution at deeper burial than their present depths of 1270–1350 m. This is in accordance with maximum burial depths of approximately 3 km for the shallow-marine deposits (Baig et al., 2016; Ktenas et al., 2019). The positive correlation between porosity and mica + feldspar can be explained by the rate of feldspar dissolution being higher than the rate of illitization. Finally, late dissolution of quartz cement and Fe-oxide precipitation probably can be attributed to uplift (Figs. 11 and 12).

6.3. Texture vs. primary composition

Although this study confirms diagenetic processes that result from deep burial and later uplift in the southwestern Barents Sea (cf. Henriksen et al., 2011), diagenesis is only a secondary effect on the reservoir qualities for the studied Lower Cretaceous deposits. Instead, our results indicate that the reservoir quality primarily was an effect of rock texture, and only to a smaller degree of composition (cf. Bjørlykke, 2014). The primary composition of sandstone is mainly governed by the tectonic situation, provenance, and climate (e.g., Dickinson and Suczek, 1979; Suttner and Dutta, 1986; Johnsson, 1990). As all studied reservoir units were deposited during greenhouse conditions (bracketing a Late Aptian-Early Albian cold phase in the Arctic; Herrle et al., 2015), and the tectonic activity barely affected the sandstone composition, the lithology in the catchments is most relevant for provenance consideration here. Particularly the high amounts of feldspar and mica that correlate with porosity in the shallow-marine facies associations and that can be related to dissolution affect the porosity, but not necessarily the permeability.

Sandstone texture resulting from the depositional conditions are shown to have affected the reservoir-quality-influencing diagenetic processes the most. The moderate clay infiltration and associated chlorite precipitation together with the moderate carbonate cementation and dissolution are effects of the texture and key diagenetic factors in enhancing the reservoir quality. This necessitates sandstone with a low content of clay clasts or pseudomatrix as for the sandstone of the slope-to-basin-floor facies associations (that commonly is better sorted than sandstone of both the shallow-marine and deltaic facies associations; Fig. 11). Similar good reservoir properties may also be expected in other areas that provided an environment of high energy, high rates of sediment supply, and access to fresh water through a physical connection between fluvial and turbidite channels at the shelf edge. On the contrary, a distal shallow-marine environment characterized by low energy

and low rates of sediment supply that only periodically is disturbed by storm events contributes to poorer sorting because of bioturbation and by allowing clay-size particles and mica grains to settle (Fig. 11). Plausibly, we could have encountered better reservoir potential for the shallow-marine sandstone than our low recorded porosity of <10% if upper shoreface deposits would have been included in the study (cf. Haile et al., 2018). Thus, both proximal shallow-marine and slope-to-basin-floor sandstone around the Loppa High may provide good reservoir quality.

7. Conclusions

This study shows that the depositional environment mainly controls the reservoir properties of Lower Cretaceous sandstone units in the southwestern Barents Sea both on microscopic (μm to cm) and local to regional (100's m to km) scale. The depositional setting is thus more important than the minor variations in (sedimentary) provenance as well as diagenesis and deep burial.

Our study shows that small compositional variations, such as different amounts of detrital feldspar and mica, can lead to different diagenetic effects in areas with similar provenance. However, most textural and compositional variations are governed by the depositional conditions under which the reservoir sand accumulated. Therefore, the porosity and permeability evolution of the various Lower Cretaceous reservoir-sandstone facies associations in the southwestern Barents Sea can be linked to specific sedimentary processes and depositional environments.

Declaration of competing interest

The authors declare that they have no known competing financial interests or personal relationships that could have appeared to influence the work reported in this paper.

Acknowledgements

We thank the LoCrA consortium (locra.uu.se) sponsors for the project support and Lundin Petroleum and Equinor for the petrographic samples supplied for this study. SAG received financial support from the Research Centre for Arctic Petroleum Exploration, funded by the Research Council of Norway (grant number 228107). We also thank Tania Hildebrand-Habel for paleontological help. Caroline Ruud, Sofie Knutdatter Arntzen, Thomas Meldahl Olsen, and Emanuela Kallesten aided with thin-section preparation and XRD analysis.

References

- Baig, I., Faleide, J.I., Jähren, J., Mondol, N.H., 2016. Cenozoic exhumation on the southwestern Barents Shelf: estimates and uncertainties constrained from compaction and thermal maturity analyses. *Mar. Petrol. Geol.* 73, 105–130.
- Basu, A., Young, S.W., Suttner, L.J., James, W.C., Mack, G.H., 1975. Re-evaluation of the use of undulatory extinction and polycrystallinity in detrital quartz for provenance interpretation. *J. Sediment. Petrol.* 45, 873–882.
- Beard, D.C., Weyl, P.K., 1973. Influence of texture on porosity and permeability of unconsolidated sand. *Am. Assoc. Petrol. Geol. Bull.* 57, 349–369.
- Beaubouef, R.T., Rossen, C., Zelt, F.B., Sullivan, M.D., Mohrig, D.C., Jennette, D.C., 1999. Deep-water sandstones, brushy canyon formation, west Texas. Field guide, hedberg field Research conference 1999. *Am. Assoc. Petroleum Geol., Continuing Educ. Course Note Ser.* 40, 1–48.
- Beaufort, D., Cassagnabere, A., Petit, S., Lanson, B., Berger, G., Lachapagne, J.C., Johansen, H., 1998. Kaolinite-to-dickite reaction in sandstone reservoirs. *Clay Miner.* 33, 297–316.
- Bhatia, M.R., Crook, K.A.W., 1986. Trace element characteristics of graywackes and tectonic setting discrimination of sedimentary basins. *Contrib. Mineral. Petrol.* 92, 181–193.
- Bjørlykke, K., 2014. Relationships between depositional environments, burial history and rock properties. Some principal aspects of diagenetic process in sedimentary basins. *Sediment. Geol.* 301, 1–14.
- Blaich, O.A., Tsikalas, F., Faleide, J.I., 2017. New insights into the tectono-stratigraphic evolution of the southern stappan high and its transition to bjørnøya basin, SW Barents Sea. *Mar. Petrol. Geol.* 85, 89–105.

- Bloch, S., Lander, R.H., Bonnell, L., 2002. Anomalously high porosity and permeability in deeply buried sandstone reservoirs: origin and predictability. *Am. Assoc. Petrol. Geol. Bull.* 86, 301–328.
- Brindley, G.W., Brown, G., 1980. Crystal structures of clay minerals and their x-ray identification. *Mineral. Soc., Lond., Monogr.* 5.
- Correns, C.W., 1978. Titanium, sections B-O. In: Wedepohl, K.H. (Ed.), *Handbook of Geochemistry 2*. Springer-Verlag, Berlin, pp. 22B1–22O17.
- Corseri, R., Faleide, T.S., Feleide, J.I., Midtkandal, I., Serck, C.S., Trulsvik, M., Planke, S., 2018. A diverted submarine channel of Early Cretaceous age revealed by high resolution seismic data, SW Barents Sea. *Mar. Petrol. Geol.* 98, 462–476.
- Dashtgard, S.E., MacEachern, J.A., Frey, S.E., Gingras, M.K., 2012. Tidal effects on the shoreline: towards a conceptual framework. *Sediment. Geol.* 279, 42–61.
- Dickinson, W.R., Suczek, C.A., 1979. Plate tectonics and sandstone compositions. *Am. Assoc. Petrol. Geol. Bull.* 63, 2164–2182.
- Dickinson, W.R., Beard, S.L., Brakenridge, R.G., Erjavec, J.L., Ferguson, R.C., Inman, K.F., Knepp, R.A., Lindberg, F.A., Ryberg, P.T., 1983. Provenance of North American Phanerozoic sandstones in relation to tectonic setting. *Geol. Soc. Am. Bull.* 94, 222–235.
- Doré, A.G., 1995. Barents Sea Geology: petroleum resources and commercial potential. *Arct. Inst. N. Am.* 48, 207–221.
- Doré, A.G., Lundin, E.R., Jensen, L.N., Birkeland, Ø., Eliassen, P.E., Fichler, C., 1999. Principal tectonic event in the evolution of the northwest European Atlantic margin. In: Fleet, A.J., Boldy, S.A.R. (Eds.), *Petroleum Geology of Northwest Europe*. Petroleum Geol. Conf. Ser., vol. 5. Geol. Soc. Lond., pp. 41–61.
- Doyle, L.J., Carder, K.L., Steward, R.G., 1983. The hydraulic equivalence of mica. *J. Sediment. Petrol.* 53, 643–648.
- Edwards, M.B., 1979. Sandstone in lower cretaceous helvetiafjellet formation, svalbard: bearing on reservoir potential of Barents shelf. *Am. Assoc. Petrol. Geol. Bull.* 63, 2193–2203.
- Ehrenberg, S.N., 1989. Assessing the relative importance of compaction processes and cementation to reduction of porosity in sandstones: discussion; compaction and porosity evolution of Pliocene sandstone, Ventura Basin, California: Discussion. *Am. Assoc. Petrol. Geol. Bull.* 73, 1274–1276.
- Ehrenberg, S.N., 1993. Preservation of Anomalously high porosity in deeply buried sandstones by grain-coating chlorite: examples from the Norwegian Continental Shelf. *Am. Assoc. Petrol. Geol. Bull.* 77, 1260–1286.
- Ehrenberg, S.N., Nadeau, P.H., 1989. formation of diagenetic illite in sandstones of the garn formation, haltenbanken area, mid-Norwegian continental shelf. *Clay Miner.* 24, 233–253.
- Enge, H.D., Howell, J.A., Buckley, S.J., 2010. Quantifying clinothem geometry in a forced-regressive river-dominated delta, Panther Tongue Member. *Utah, USA. Sediment* 57, 1750–1770.
- Engelhardt, W.V., 1960. *Der Porenraum der Sedimente*. Springer-Verlag, Berlin.
- Faleide, J.I., Vågnes, E., Gudlaugsson, S.T., 1993. Late Mesozoic-Cenozoic evolution of the southwestern Barents Sea in a regional rift-shear tectonic setting. *Mar. Petrol. Geol.* 10, 186–214.
- Faleide, J.I., Pease, V., Curtis, M., Klitzke, P., Minakov, A., Scheck-Wenderoth, M., Kostyuchenko, S., Zayonchek, A., 2018. Tectonic implications of the lithospheric structure across the Barents and Kara shelves. In: Pease, V., Coakley, B. (Eds.), *Circum-Arctic Lithosphere Evolution*. Geol. Soc., Lond., vol. 460. , Special Publ, pp. 285–314.
- Fedo, C.M., Nesbitt, H.W., Young, G.M., 1995. Unraveling the effects of potassium metasomatism in sedimentary rocks and paleosols, with implications for paleoweathering conditions and provenance. *Geol.* 23, 921–924.
- Gabrielsen, R.H., Færseth, R.B., Jensen, L.N., Kalheim, J.E., Riis, F., 1990. Structural elements of the Norwegian continental shelf. Part I: the Barents Sea region. *Nor. Petroleum Dir. Bull.* 6, 1–33.
- Gani, R.R., Bhattacharya, J.P., 2005. Lithostratigraphy versus chronostratigraphy in facies correlations of quaternary deltas: application of bedding correlation. In: Giosan, L., Bhattacharya, J.P. (Eds.), *River Deltas – Concepts, Models, and Examples*, vol. 83. SEPM Special Publ, pp. 31–47.
- Gaupp, R., Okkerman, J.A., 2011. Diagenesis and reservoir quality of Rotliegend sandstones in the northern Netherlands—a review. In: Grötsch, J., Gaupp, R. (Eds.), *The Permian Rotliegend of the Netherlands*, vol. 98. SEPM Special Publ, pp. 193–226.
- Gobo, K., Ghinassi, M., Nemeč, W., 2015. Gilbert-type deltas recording short-term base-level changes: delta-brink morphodynamics and related foreset facies. *Sediment* 62, 1923–1949.
- Grundvåg, S.-A., Marín, D., Kairanov, B., Śliwińska, K.K., Nøhr-Hansen, H., Jelby, M.E., Escalona, A., Olaussen, S., 2017. The lower cretaceous succession of the northwestern Barents shelf onshore and offshore correlations. *Mar. Petrol. Geol.* 86, 834–857.
- Gutiérrez Paredes, H.C., Catuneanu, O., Hernández Romano, U., 2018. Controls on the quality of Miocene reservoirs, southern Gulf of Mexico. *J. S. Am. Earth Sci.* 81, 45–65.
- Haile, B.G., Klausen, T.G., Czarniecka, U., Xi, K., Jahren, J., Hellevang, H., 2018. How are diagenesis and reservoir quality linked to depositional facies? A deltaic succession, Edgeøya, Svalbard. *Mar. Petrol. Geol.* 92, 519–546.
- Halland, E.K., Bjørnstad, A., Gjeldvik, I.T., Bjørheim, M., Magnus, C., Meling, I.M., Mujezinović, J., Riis, F., Rod, R.S., Pham, V.T.H., Tappel, I., 2014. The Barents Sea. In: Halland, E., Mujezinović, J., Riis, F. (Eds.), *CO₂ Storage Atlas - Norwegian Continental Shelf*. Nor. Petroleum Dir. Stavanger, pp. 107–145.
- Henriksen, E., Bjørnseth, H.M., Hals, T.K., Heide, T., Kiryukhina, T., Kløvjan, O.S., Larssen, G.B., Ryseth, A.E., Rønning, K., Sollid, K., Stoupakova, A., 2011. Uplift and erosion of the greater Barents Sea: impact on prospectivity and petroleum systems. In: Spencer, A.M., Embry, A.F., Gautier, D.L., Stoupakova, A.V., Sørensen, K. (Eds.), *Arctic Petroleum Geology*. Geol. Soc., Lond., Mem., vol. 35, pp. 271–281.
- Herrle, J.O., Schröder-Adams, C.J., Davis, W., Pugh, A.T., Galloway, J.M., Fath, J., 2015. Mid-cretaceous high arctic stratigraphy, climate, and oceanic anoxic events. *Geol.* 43, 403–406.
- Houseknecht, D.W., Ross, L.M., 1992. Clay minerals in Atokan deep-water sandstone facies, Arkoma basin: origins and influence on diagenesis and reservoir quality. In: Houseknecht, D.W., Pittman, E.D. (Eds.), *Origin, Diagenesis, and Petrophysics of Clay Minerals in Sandstones*, vol. 47. SEPM Special Publ, pp. 227–240.
- Indrevær, K., Gabrielsen, R.H., Faleide, J.I., 2017. Early Cretaceous synrift uplift and tectonic inversion in the Loppa High area, southwestern Barents Sea, Norwegian shelf. *J. Geol. Soc.* 174, 242–254.
- Iqbal, J., 2016. Reservoir Characterization of the Lower Cretaceous Clastic Wedges in the Southwestern Barents Sea Using Seismic Analysis and Rock Physics Diagnostic. MSc thesis, University of Stavanger, Norway.
- Jakobssen, M., Mayer, L., Coakley, B., Dowdeswell, J.A., Forbes, S., Fridman, B., Hodnesdal, H., Noormets, R., Pedersen, R., Rebescio, M., 2012. The international bathymetric chart of the Arctic Ocean (IBCAO) version 3.0. *Geophys. Res. Lett.* 39 <https://doi.org/10.1029/2012GL052219> paper L12609.
- Johnsson, M.J., 1990. Tectonic versus chemical-weathering controls on the composition of fluvial sands in tropical environments. *Sediment* 37, 713–726.
- Kairanov, B., Marín, D., Escalona, A., Cardozo, N., 2019. Growth and linkage of a basin-bounding fault system: insights from the early cretaceous evolution of the northern polhem subplatform, SW Barents Sea. *J. Struct. Geol.* 124, 182–196.
- Ketzer, J.M., Morad, S., 2006. Predictive distribution of shallow marine, low-porosity (pseudomatrix-rich) sandstones in a sequence stratigraphic framework – example from the Ferron sandstone, Upper Cretaceous, USA. *Mar. Petrol. Geol.* 23, 29–36.
- Ktenas, D., Meisingset, I., Henriksen, E., Nielsen, J.K., 2019. Estimation of net apparent erosion in the SW Barents Sea by applying velocity inversion analysis. *Petrol. Geosci.* 25, 169–187.
- Lien, T., Midtbø, R.E., Martinsen, O.J., 2006. Depositional facies and reservoir quality of deep-marine sandstones in the Norwegian Sea. *Nor. J. Geol.* 86, 71–92.
- Lowe, D.R., 1982. Sediment gravity flows: II. Depositional models with special reference to the deposits of high-density turbidity currents. *J. Sediment. Petrol.* 52, 279–297.
- Lowenmark, L., 2007. Importance and usefulness of trace fossils and bioturbation in paleoceanography. In: Miller, W. (Ed.), *Trace Fossils: Concepts, Problems, Prospects*. Elsevier, Amsterdam, pp. 404–418.
- MacEachern, J.A., Bann, K.L., 2008. The role of ichnology in refining shallow marine facies models. In: Hampson, G.J., Steel, R.J., Burgess, P.M., Dalrymple, R.W. (Eds.), *Recent Advances in Models of Siliciclastic Shallow-Marine Stratigraphy*, vol. 90. Soc. Sediment. Geol., Special Publ, pp. 73–116.
- Mansurbeg, H., El-ghali, M.A.K., Morad, S., Plink-Björklund, P., 2006. The impact of meteoric water on the diagenetic alterations in deep-water, marine siliciclastic turbidites. *J. Geochem. Explor.* 89, 254–258.
- Mansurbeg, H., Morad, S., Al Suwaidi, M., Qurtas, S., Tveiten, O.G., Shahrokhizadeh, S., Harchegani, F.K., 2020. Meteoric-water incursion into marine turbiditic sandstones: evidence from the andrew formation (paleocene), UK central gulf, north sea. *Mar. Petrol. Geol.* 118 <https://doi.org/10.1016/j.marpetgeo.2020.104428> paper 104428.
- Marín, D., Escalona, A., Śliwińska, K.K., Nøhr-Hansen, H., Mordasova, A., 2017. Sequence stratigraphy and lateral variability of Lower Cretaceous clinoforms in the southwestern Barents Sea. *Am. Assoc. Petrol. Geol. Bull.* 101, 1487–1517.
- Marín, D., Escalona, A., Grundvåg, S.-A., Nøhr-Hansen, H., Kairanov, B., 2018a. Effects of adjacent fault systems on drainage patterns and evolution of uplifted rift shoulders: the Lower Cretaceous in the Loppa High, southwestern Barents Sea. *Mar. Petrol. Geol.* 94, 212–229.
- Marín, D., Escalona, A., Grundvåg, S.-A., Olaussen, S., Sandvik, S., Śliwińska, K.K., 2018b. Unravelling key controls on the rift climax to post-rift fill of marine rift basins: insights from 3D seismic analysis of the Lower Cretaceous of the Hammerfest Basin, SW Barents Sea. *Basin Res.* 30, 587–612.
- Matlack, S., Houseknecht, D.W., Applin, K.R., 1989. Emplacement of clay into sand by infiltration. *J. Sediment. Petrol.* 59, 77–87.
- McBride, E.F., 1963. A classification of common sandstones. *J. Sediment. Petrol.* 33, 664–669.
- McLennan, S.M., Taylor, S.R., McCulloch, M.T., Maynard, J.B., 1990. Geochemical and Nd-Sr isotopic composition of deep-sea turbidites: crustal evolution and plate tectonic associations. *Geochem. Cosmochim. Acta* 54, 2015–2050.
- McLennan, S.M., Hemming, S., McDaniel, D.K., Hanson, G.N., 1993. Geochemical approaches to sedimentation, provenance, and tectonics. In: Johnsson, M.J., Basu, A. (Eds.), *Processes Controlling the Composition of Clastic Sediments*, vol. 284. Geol. Soc. Am., Special Pap, pp. 21–40.
- Midtkandal, I., Faleide, J.I., Faleide, T.S., Serck, C.S., Planke, S., Corseri, R., Dimitriadis, M., Nystuen, J.P., 2020. Lower Cretaceous Barents Sea strata: epicontinental basin configuration, timing, correlation and depositional dynamics. *Geol. Mag.* 157, 458–476.
- Milliken, K.L., McBride, E.F., Cavazza, W., Cibin, U., Fontana, D., Picard, M.D., Zuffa, G. G., 1998. Geochemical history of calcite precipitation in Tertiary sandstones, northern Apennines, Italy. In: Morad, S. (Ed.), *Carbonate Cementation in Sandstones: Distribution Patterns and Geochemical Evolution*. Blackwell Science, Oxford, pp. 213–239.
- Moore, D.M., Reynolds Jr., R.C., 1997. X-ray Diffraction and the Identification and Analysis of Clay Minerals, vol. 2. Oxford University Press, New York.
- Morad, S., Al-Ramadan, K., Ketzer, J.M., De Ros, L.F., 2010. The impact of diagenesis on the heterogeneity of sandstone reservoirs: a review of the role of depositional facies and sequence stratigraphy. *Am. Assoc. Petrol. Geol. Bull.* 94, 1267–1309.
- Moraes, M.A.S., De Ros, L.F., 1990. Infiltrated clays in fluvial Jurassic sandstones of Recôncavo Basin, northeastern Brazil. *J. Sediment. Petrol.* 60, 809–819.

- Moraes, M.A.S., DeRos, L.F., 1992. Depositional, infiltrated clays in fluvial sandstones of the jurassic sergi formation, recôncavo basin, northeastern Brazil. *SEPM (Soc. Sediment. Geol.) Spec. Publ.* 47, 197–208.
- Mørk, A., Dallman, W.K., Dypvik, H., Johannessen, E.P., Larssen, G.B., Nagy, J., Nøttvedt, A., Olausen, S., Pêlina, T.M., Worsley, D., 1999. Mesozoic lithostratigraphy. In: Dallmann, W.K. (Ed.), *Lithostratigraphic Lexicon of Svalbard. Review and Recommendations for Nomenclature Use: Upper Palaeozoic to Quaternary Bedrock*. Nor. Polarinst. Tromsø, pp. 127–214.
- Mørk, M.B.E., 1999. Compositional variations and provenance of triassic sandstones from the Barents shelf. *J. Sediment. Res.* 69, 690–710.
- Mutti, E., Ricci Lucchi, F., 1972. Turbidites of the northern Apennines: introduction to facies analysis. *Int. Geol. Rev.* 20, 125–166.
- Nøhr-Hansen, H., 1993. Dinoflagellate cyst stratigraphy of the barremanian to albian, lower cretaceous, east Greenland. *Grøn. Geol. Unders. Bull.* 166, 1–171.
- Ohkouchi, N., Kuroda, J., Taira, A., 2015. The origin of Cretaceous black shales: a change in the surface ocean ecosystem and its trigger. *Proc. Jpn. Acad. Ser. B Phys. Biol. Sci.* 91, 273–291.
- Pittman, E.D., Larese, R.E., Heald, M.T., 2010. Clay coats: occurrence and relevance to preservation of porosity in sandstones. In: Houseknecht, D.W., Pittman, E.D. (Eds.), *Origin, Diagenesis, and Petrophysics of Clay Minerals in Sandstones*, vol. 47. *SEPM Special Publ.* pp. 241–255.
- Prochnow, E.A., Remus, M.V.D., Ketzner, J.M., Gouveia Jr., J.C.R., Schiffer de Souza, R., De Ros, L.F., 2006. Organic – inorganic interactions in oilfield sandstones: examples from turbidite reservoirs in the Campos Basin, offshore eastern Brazil. *J. Petrol. Geol.* 29, 361–380.
- Qin, Y.-C., Xue, C., Jiang, X., 2018. Tidal current-dominated depositional environments in the central-northern Yellow Sea as revealed by heavy-mineral and grain-size dispersals. *Mar. Petrol. Geol.* 398, 59–72.
- Raiswell, R., 1987. Non-steady state microbiological diagenesis and the origin of concretions and nodular limestones. In: Marshall, J.D. (Ed.), *Diagenesis of Sedimentary Sequences*. *Geol. Soc., Lond.*, vol. 36. , Special Publ., pp. 41–54.
- Ramm, M., 2000. Reservoir quality and its relationship to facies and provenance in Middle to Upper Jurassic sequences, northeastern North Sea. *Clay Miner.* 35, 77–94.
- Reed, J.S., Eriksson, K.A., Kowalewski, M., 2005. Climatic, depositional and burial controls on diagenesis of Appalachian Carboniferous sandstones: qualitative and quantitative methods. *Sediment. Geol.* 176, 225–246.
- Richardson, G., Vorren, T.O., Tørudbakken, B.O., 1993. Post-Early Cretaceous uplift and erosion in the southern Barents Sea: a discussion based on analysis of seismic interval velocities. *Nor. Geol. Tidsskr.* 73, 3–20.
- Sattar, N., Juhlin, C., Koyi, H., Ahmad, N., 2017. Seismic stratigraphy and hydrocarbon prospectivity of the lower cretaceous Knurr sandstone lobes along the southern margin of Loppa high, Hammerfest basin, Barents Sea. *Mar. Petrol. Geol.* 85, 54–69.
- Sayago, J., Di Lucia, M., Mutti, M., Cotti, A., Sitta, A., Broberg, K., Przybylo, A., Buonaguro, R., Zimina, O., 2012. Characterization of a deeply buried paleokarst terrain in the Loppa High using core data and multiattribute seismic facies classification. *Am. Assoc. Petrol. Geol. Bull.* 96, 1843–1866.
- Seilacher, A., 1967. Bathymetry of trace fossils. *Mar. Geol.* 5, 413–428.
- Seldal, J., 2005. Lower Cretaceous: the next target for oil exploration in the Barents Sea?. In: Doré, A.G., Vining, B.A. (Eds.), *Petroleum Geology: North-West Europe and Global Perspectives*. *Geol. Soc., Lond.*, vol. 6. *Petroleum Geol. Conf. Ser.*, 321–240.
- Serck, C.S., Faleide, J.L., Braathen, A., Kjølhamar, B., Escalona, A., 2017. Jurassic to early Cretaceous basin configuration(s) in the Fingerdjupet Subbasin, SW Barents Sea. *Mar. Petrol. Geol.* 86, 874–891.
- Shanmugam, G., Moila, R.J., Damuth, J.E., 1985. Eustatic control of submarine fan development. In: Bouma, A.H., Normark, W.R., Barnes, N.E. (Eds.), *Submarine Fans and Related Turbidite Systems*. Springer-Verlag, New York, pp. 23–28.
- Shanmugam, G., Lehtonen, L.R., Straume, T., Syvertsen, S.E., Hodgkinson, R.J., Skibeli, M., 1994. Slump and debris-flow dominated upper slope facies in the Cretaceous of the Norwegian and northern North seas (61–67°N): implications for sand distribution. *Am. Assoc. Petrol. Geol. Bull.* 78, 910–937.
- Stemmerik, L., Elvebak, G., Worsley, D., 1999. Upper Palaeozoic carbonate reservoirs on the Norwegian Arctic Shelf: delineation of reservoir models with application to the Loppa High. *Petrol. Geosci.* 5, 173–187.
- Stewart, D.J., Berge, K., Bowlin, B., 1995. Exploration trends in the southern Barents Sea. In: Hanslien, S. (Ed.), *Petroleum Exploration and Exploitation in Norway*, vol. 4. *NPF Special Publ.* pp. 253–276.
- Suttner, L.J., Dutta, P.K., 1986. Alluvial sandstone composition and paleoclimate, I. Framework mineralogy. *J. Sediment. Petrol.* 56, 329–245.
- Taylor, A.M., Goldring, R., 1993. Description and analysis of bioturbation and ichnofabric. *J. Geol. Soc., Lond.* 150, 141–148.
- Taylor, S.R., McLennan, S.M., 1985. *The Continental Crust: its Composition and Evolution*. Blackwell, Oxford.
- Tortosa, A., Palomares, M., Arribas, J., 1991. Quartz grain types in Holocene deposits from the Spanish Central System: some problems in provenance analysis. In: Morton, A.C., Todd, S.P., Haughton, P.D.W. (Eds.), *Developments in Provenance Studies*. *Geol. Soc., Lond.*, vol. 57. , Special Publ., pp. 47–54.
- Velde, B., 2003. Green clay minerals. In: Mackenzie, F.T. (Ed.), *Sediments, Diagenesis, and Sedimentary Rocks, Treatise on Geochem*, vol. 7, pp. 309–324.
- Walker, T.R., 1976. Diagenetic origin of continental red beds. In: Falke, H. (Ed.), *The Continental Permian in Central, West and South Europe*. *NATO ASI Series, Series C: Math.* vol. 22. . *Phys. Sci.*, pp. 240–282.
- Worden, R.H., Morad, S., 2003. Clay minerals in sandstones: controls on formation, distribution and evolution. *Int. Assoc. Sedimentol. Special Publ.* 34, 3–41.
- Worsley, D., 2008. The post-Caledonian development of Svalbard and the western Barents Sea. *Polar Res.* 27, 298–317.
- Yang, Z., He, S., Wang, F., He, Z., Wu, H., Meng, X., 2009. Carbonate cementation-dissolution in deep-seated sandstones near the overpressure top in central Junggar Basin, Xinjiang, NW China. *Chin. J. Geochem.* 28, 86–96.